THE JOURNAL OF BIOLOGICAL CHEMISTRY VOL. 287, NO. 39, pp. 32897–32912, September 21, 2012

Dynamic Structural Changes Are Observed upon Collagen and Metal Ion Binding to the Integrin α1 I Domain*

Received for publication, February 17, 2012, and in revised form, July 11, 2012 Published, JBC Papers in Press, July 30, 2012, DOI 10.1074/jbc.M112.354365

Paul H. Weinreb[‡1,2], Sheng Li[§1], Sharon X. Gao[‡], Tong Liu[§], R. Blake Pepinsky[‡], Justin A. Caravella[‡], Jun H. Lee[§], and Virgil L. Woods, Jr.[§3]

From [‡]Biogen Idec, Inc., Cambridge, Massachusetts 02142 and the [§]Department of Medicine and Biomedical Sciences Graduate Program, University of California San Diego, La Jolla, California 92093-0656

Background: Integrin α1 I domain undergoes conformational changes upon collagen binding.
Results: Deuterium exchange was used to measure the effects of cations, collagen, or an antibody on the α1I solution structure.
Conclusion: Full-length collagen and metal ions induce changes that differ in key aspects from previously proposed models for α1I activation.
Significance: These studies support a new model for integrin I domain activation.

We have applied hydrogen-deuterium exchange mass spectrometry, in conjunction with differential scanning calorimetry and protein stability analysis, to examine solution dynamics of the integrin α1 I domain induced by the binding of divalent cations, full-length type IV collagen, or a function-blocking monoclonal antibody. These studies revealed features of integrin activation and α1I-ligand complexes that were not detected by static crystallographic data. Mg^{2+} and Mn^{2+} stabilized α1I but differed in their effects on exchange rates in the αC helix. Ca^{2+} impacted α1I conformational dynamics without altering its gross thermal stability. Interaction with collagen affected the exchange rates in just one of three metal ion-dependent adhesion site (MIDAS) loops, suggesting that MIDAS loop 2 plays a primary role in mediating ligand binding. Collagen also induced changes consistent with increased unfolding in both the αC and allosteric C-terminal helices of α1I. The antibody AQC2, which binds to α1I in a ligand-mimetic manner, also reduced exchange in MIDAS loop 2 and increased exchange in αC, but it did not impact the C-terminal region. This is the first study to directly demonstrate the conformational changes induced upon binding of an integrin I domain to a full-length collagen ligand, and it demonstrates the utility of the deuterium exchange mass spectrometry method to study the solution dynamics of integrin/ligand and integrin/metal ion interactions. Based on the ligand and metal ion binding data, we propose a model for collagen-binding integrin activation that explains the differing abilities of Mg^{2+}, Mn^{2+}, and Ca^{2+} to activate I domain-containing integrins.

Because of their critical role in mediating cell/cell and cell/matrix interactions, integrins are among the most studied families of transmembrane receptors. In particular, great progress has been made in understanding the general structural features of these heterodimeric cell-surface receptors and the conformational changes that regulate affinity modulation, ligand binding, and signaling (1, 2). Crystal structures of both intact integrins and functional domains have been critical to this process. Of particular interest is the α subunit I domain that is primarily responsible for mediating ligand binding by integrins containing this domain. Among others, the co-crystal structures of disulfide-"locked" αL I domains with ICAM-1 (3), ICAM-3 (4), and ICAM-5 (5) and the α2 I domain (α2I) with a collagen triple-helical peptide (THP)[4] (6) have provided snapshots of the closed (nonligand bound), open (ligand-bound), and intermediate conformations of the ligand-binding regions of these integrins. In many cases, direct structural comparisons between free and ligand-bound integrins (or integrin I domains) cannot be made on the basis of existing data. Even less data are available on the nature of the conformational changes that occur upon integrin-ligand binding in solution. Thus, it is important to develop solution-based methods that allow the direct assessment of the conformational dynamics of integrin/ligand interactions.

In humans, the 18 α and 8 β integrin subunits pair to form at least 24 known heterodimers (7). Nine of the α subunits contain I domains, which play a central role in ligand binding and selectivity. The four collagen-binding receptors (α1β1, α2β1, α10β1, and α11β1) fall into this subset of I domain-containing integrins. Of these, α1β1 (VLA1) and α2β1 (VLA2) have been the most thoroughly studied. The crystal structure of α2I has been determined in the presence of a heterotrimeric THP corresponding to its primary ligand, type I collagen (6). These studies, along with structural studies of the α I domains of the β2

* This work was supported, in whole or in part, by National Institutes of Health Grants CA099835, CA118595, AI076961, AI072106, AI068730, AI081982, AI2008031, GM037684, GM020501, GM066170, GM093325, NS070899, and RR029388. This work was also supported by Discovery Grant UC10591 from the University of California IUCRP Program, Biogen Idec corporate sponsor (to V. L. W.).

[1] Both authors contributed equally to this work.

[2] To whom correspondence may be addressed: Biogen Idec, Inc., 14 Cambridge Center, Cambridge, MA 02142. Tel.: 617-679-2351; Fax: 617-679-3148; E-mail: paul.weinreb@biogenidec.com.

[3] To whom correspondence may be addressed: Dept. of Medicine and Biomedical Sciences Graduate Program, University of California San Diego, 9500 Gilman Dr., MC 0656, La Jolla, CA 92093-0656. Tel.: 619-708-2449; Fax: 858-534-2180; E-mail: vwoods@ucsd.edu.

[4] The abbreviations used are: THP, collagen triple-helical peptide; VLA1, very late antigen-1 (α1β1 integrin); VLA2; very late antigen-2 (α2β1 integrin); MIDAS, metal ion-dependent adhesion site; DXMS, hydrogen-deuterium exchange mass spectrometry; DSC, differential scanning calorimetry; GdnHCl, guanidine hydrochloride; ND, nondeuterated; D/D, hydrogen-deuterium.

integrins LFA-1 (4, 5, 8–11), Mac-1 (12, 13), and αXβ2 (14), have helped to establish and refine a model for the ligand-induced conformational changes that lead to "outside-in" signaling in I domain-containing integrins (1). In this model, ligand binding to the divalent cation within the I domain metal ion-dependent adhesion site (MIDAS) induces a shift from the so-called "closed" (unliganded) to the "open" (liganded) conformation and induces allosteric changes in the C-terminal α7 helix of the I domain, triggering a large scale rearrangement of the global topology of the receptor. This model was refined to include the concept of an "intrinsic ligand," in which a glutamate from the C terminus of the I domain binds to the MIDAS site within a similar domain within the β subunit (the β I domain or "I-like" domain) (15, 16).

VLA1 is a major receptor for basement membrane-type IV collagen and is expressed on hematopoietic, neuronal, and mesenchymal cell types (17). Inhibition of VLA1 function, through the use of genetic knock-outs or pharmacological agents, blocks cell retention and activation in pathogenic sites and leads to reduced inflammation and amelioration of disease in a variety of animal models (for examples, see Refs. 18–25). Despite the wealth of biological and pharmacological data on VLA1, limited structural information is available for this integrin. Crystal structures of isolated α1 I domains (α1I) have been reported (26–28), as well as the structure of α1I in complex with the function-blocking antibody AQC2 (29, 30). Although computational models have been proposed for the α1I open conformation (27) and for the α1I/collagen interaction site (31), no structures of α1I in complex with any type of ligand or ligand-mimetic peptide have been reported (2). Recently, the structure of α1I containing an activating mutation (E317A) was determined (32). This protein adopted a novel conformation that differed from both the open and closed structures previously published for other integrins, indicating that the activation mechanism of collagen-binding integrins may differ from that of other integrins.

Peptide amide hydrogen-deuterium exchange mass spectrometry (DXMS) has been used to analyze protein/protein, protein/substrate, protein/inhibitor, protein/solvent, and protein/DNA interactions, as well as protein dynamics and protein conformational changes (33–40). Here, we utilized DXMS to directly study the solution binding and conformational dynamics of the interaction between α1I and full-length type IV collagen. DXMS allowed us to investigate the conformational changes that occur when α1I binds to collagen under conditions closely resembling the native physiological environment and to test the current structural models for integrin I domain/ligand interactions that are largely based on static crystallographic data. We also examined conformational changes induced upon binding of the function-blocking α1 monoclonal antibody AQC2 and compared them with those mediated by the native ligand. Our results reveal important differences from existing models for integrin I domain/ligand interactions and ligand-induced allosteric changes, and they suggest novel dynamic features of the α1I/collagen and α1I/metal ion interactions. The methods we developed to characterize the α1I domain should be easily adapted to the study of other integrins.

EXPERIMENTAL PROCEDURES

Protein Preparation—These studies utilized a chimeric α1I comprising elements of both the rat and human sequences (Fig. 1). The sequence numbering is based on the full-length mature human α1 integrin sequence (NCBI Reference Sequence NP_852478.1). Four human residues (Val-213, Gln-214, Arg-215, and Arg-218) were substituted into the MIDAS region of the corresponding rat α1I sequence. This form of α1I was used to establish the binding sites for anti-human α1 integrin antibodies using biochemical methods (41) and was crystallized in complex with a Fab fragment of the function-blocking anti-human α1 integrin antibody AQC2 (29, 30). The bacterially expressed chimeric α1I is significantly more soluble than its fully human GST-α1I fusion counterpart, making it more suitable for structural studies. Recombinant α1I was expressed in *Escherichia coli* as a glutathione *S*-transferase (GST) fusion protein and was purified as described previously (41). Samples were analyzed using size exclusion chromatography on a Superdex 200 10/300 GL column using phosphate-buffered saline (PBS) as the mobile phase and compared with a reference standard mixture (Bio-Rad). For studies requiring removal of the GST tag, the protein was cleaved using thrombin and purified as described previously (41). The anti-α1β1 monoclonal antibody AQC2 was prepared as described previously (41).

Ligand Binding Studies—The binding of GST-α1I to collagen was measured using an electrochemiluminescence assay (42). Type IV collagen from human placenta (Sigma) was coated onto Tosyl M-280 Dynabeads (Dynal, A.S., Oslo, Norway) at a ratio of 20 μg of collagen/mg of beads, as described previously (42). Beads were blocked by incubation with 8% rat plasma in assay buffer (50 mM Hepes, pH 7.5, 150 mM NaCl, 0.1% Triton X-100) for 15 min at 25 °C prior to use. A goat polyclonal antibody against GST (GE Healthcare) was labeled with ruthenium(II) tris(bipyridine)-NHS ester (TAG-NHS Ester; IGEN International, Inc., Gaithersburg, MD) as per the manufacturer's instructions. Serial dilutions of GST-α1I in assay buffer were incubated with 30 μg/ml labeled anti-GST antibody, 0.2 mg/ml collagen-coated beads, and 0.5 mM $MnCl_2$, in a final volume of 120 μl. After gentle agitation at 25 °C for 60 min, 200 μl of assay buffer was added, and samples were read in an ORIGEN 5.1 detector according to the manufacturer's instructions (IGEN). To assess the blocking ability of AQC2, serial dilutions of AQC2 were incubated with 5 ng/ml GST-α1I, 2 μg/ml labeled anti-GST antibody, 0.2 mg/ml collagen-coated beads, and 1 mM $MnCl_2$ in a final volume of 100 μl and processed as described above.

Differential Scanning Calorimetry—DSC was performed using an automated capillary DSC (capDSC, GE Healthcare). Protein and reference solutions were sampled automatically from 96-well plates using the robotic attachment. Prior to each sample measurement, two buffer scans were performed to define the base line for subtraction. All 96-well plates containing protein were stored within the instrument at 5 °C. Each I domain sample was diluted to 1 mg/ml in relevant buffer. Scans were performed from 10 to 100 °C at 2 °C/min using the high feedback mode for enhanced peak resolution. Scans were analyzed using the Origin software package supplied by the manu-

facturer. Subsequent to the subtraction of reference base-line scans, nonzero sample base lines were corrected using a third order polynomial. The unfolding parameters for the multidomain unfolding profiles of I domain were deconvoluted using the multipeak fitting routine within the software assuming non-two-state unfolding behavior. The measured melting temperature (T_m) for α1I in the presence of the chelating agent EDTA ranged from 54.5 to 57.9 °C, depending on the protein concentration, buffer composition, and scan rate, but it was reproducible ±1 °C within a given set of experimental parameters.

Denaturation Studies—The denaturation of α1I as a function of urea was measured by fluorescence spectroscopy (41). Briefly, samples containing 300 μg/ml α1I in 50 mM Tris-HCl, pH 7.5, 0.1 mM DTT with 10 mM EDTA, 10 mM $CaCl_2$, or 1 mM $MnCl_2$ and with varying amounts of urea were analyzed at 25 °C using an excitation wavelength of 280 nm. Emission spectra from 300 to 400 nm were collected using a Spectramax M5 fluorescence spectrometer (Molecular Devices Inc., Sunnyvale, CA). Fluorescence data at 350 nm were plotted as a function of urea and standardized using the change in fluorescence from 0 to 9 M urea for each of the test conditions as a measure of the total fraction folded.

Optimization of Fragmentation Conditions—Prior to conducting the hydrogen-deuterium exchange experiments, test digests prepared with undeuterated buffer in varying concentrations of guanidine hydrochloride (GdnHCl) were made to optimize proteolysis conditions for the best peptide coverage (43). For each sample, 6 μl of stock solution of α1 I domain (8 mg/ml) was first diluted with 18 μl of H_2O buffer (150 mM NaCl, 8.3 mM Tris-HCl, pH 7.2). The sample was then quenched with 36 μl of a quench solution (0 °C) of 0.8% formic acid, 17% glycerol, and GdnHCl at final concentrations of 0.05, 0.5, 1.0, 2.0, or 4.0 M. This quenching step lowered the pH to 2.2–2.5 to minimize further hydrogen-deuterium exchange in subsequent deuterated samples. The quench-denaturation process was allowed to proceed on ice for 30 s, after which the sample was stored frozen at −80 °C. Procedures for pepsin digestion for DXMS have been described previously (44–48). Briefly, a sample was thawed at 5 °C and then immediately digested over a protease column (66-μl bed volume) filled with porcine pepsin (Sigma; immobilized on Poros 20 AL medium at 30 mg/ml following the manufacturer's instructions) at a flow rate of 100 μl/min with 0.05% trifluoroacetic acid. Peptic fragments were collected on a C18 trap column and separated on a C18 reversed phase column (Vydac, catalog no. 218MS5105) with a linear acetonitrile gradient from 6 to 38%. The column effluent was electrosprayed directly into an LCQ Classic (Thermo Finnigan, Inc.) or Q-TOF mass spectrometer (Micromass). Determination of pepsin-generated peptides from MS/MS data sets was facilitated through the use of SEQUEST (Thermo Finnigan, Inc.). This set of peptides was then further verified by DXMS Explorer (Sierra Analytics Inc., Modesto, CA). The peptide coverage maps for the different concentrations of GdnHCl were compared, and the condition with the best coverage map for each individual protein or protein complex was used for subsequent deuterium exchange experiments.

Hydrogen-Deuterium Exchange Experiments—Samples were prepared with three states of hydrogen-deuterium exchange as follows: nondeuterated (ND), partially deuterated, and equilibrium deuterated. All samples were processed as described above. Equilibrium deuterated samples were prepared by incubating protein at room temperature in D_2O buffer (1% (v/v) formic acid) overnight. Procedures for individual experiments are described below. The hydrogen-deuterium exchange experiments performed with our automated apparatus produces measurements of deuteron incorporation where the standard deviation is less than 2% of the mean of triplicate determinations (49, 50).

α1 I Domain—α1 I domain solutions (8 mg/ml) were mixed with solutions of $CaCl_2$, $MnCl_2$, or EDTA to final concentrations of 1, 0.5, or 5 mM, respectively, or with $MgCl_2$ at either 1 or 10 mM. The solutions were preincubated at room temperature for 10 min and then chilled to 0 °C. The ND sample was processed exactly as described under "Optimization of Fragmentation Conditions." Hydrogen-deuterium exchange experiments were initiated by mixing 6 μl of preincubated samples with 18 μl of D_2O buffer (8.3 mM Tris, 150 mM NaCl, pH 7.2, in D_2O). The samples with 10 mM Mg^{2+} were incubated at 0 °C for 10, 30, or 100 s or at 25 °C for 30, 100, or 300 s. All other samples were incubated at 0 °C for 10, 30, or 300 s or at 25 °C for 30, 100, 300, 1000, 3000, 10,000, 30,000, 100,000, or 300,000 s. At the indicated times, the H/D exchange was quenched by adding 36 μl of ice-cold quench solution (0.8% formic acid, 16.6% glycerol, and 0.05 M GdnHCl). The samples were then transferred to ice-cooled autosampler vials, frozen on dry ice, and stored at −80 °C. As shown in previous studies (51–54), incubation at 0 °C for 10, 30, or 100 s is equivalent to incubation at 25 °C for 1, 3, or 10 s, respectively. For all ribbon diagrams, the data generated at 0 °C were converted to the data equivalent at 25 °C.

AQC2-α1 I Domain Complex—The complex between antibody AQC2 and α1I was prepared by mixing solutions of α1I (7 mg/ml) and antibody (6.4 mg/ml) at a 2:1 molar ratio at room temperature for 30 min and then chilling to 0 °C. The ND sample was processed by diluting 25 μl of the complex with 75 μl of H_2O Buffer (8.3 mM Tris, 150 mM NaCl, pH 7.2) and then mixed with 100 μl of quench solution (0.8% formic acid, 16.6% glycerol, 0.5 M GdnHCl). For deuterated samples, 25 μl of preincubated sample was mixed with 75 μl of D_2O buffer and incubated at various time intervals (10, 30, and 100 s at 0 °C and 30, 100, 300, 1000, 3000, 10,000, 30,000, 100,000, and 300,000 s at 25 °C) before being added to 100 μl of quench solution. All samples were frozen on dry ice. Incubation at 0 °C for 10, 30, or 100 s is equivalent to incubation at 25 °C for 1, 3, or 10 s, respectively.

GST-α1 I Domain—For the ND sample, 5 μl of GST-α1I (12.7 mg/ml with 10 mM $MgCl_2$) was diluted with 64 μl of H_2O buffer and quenched with 96 μl of quench solution (0.8% formic acid, 16.6% glycerol, 0.5 M GdnHCl). Deuterated samples were prepared by diluting 5 μl of GST-α1I with 11 μl of H_2O buffer, followed by mixing with 48 μl of D_2O buffer. Samples were incubated for 10, 100, and 1000 s at 0 °C and 300, 1000, 3000, 10,000, 30,000, and 100,000 s at 25 °C. At the indicated times, the samples were added to vials containing the 96 μl of quench solution. The samples were transferred to autosampler vials

and frozen on dry ice. Incubation at 0 °C for 10, 100, or 300 s is equivalent to incubation at 25 °C for 1, 10, or 100 s, respectively.

GST-α1 I Domain-Collagen Complex—An on-column exchange process was used to eliminate the interference of collagen peptides during data acquisition. The collagen column was created by the following procedure: 5 mg of collagen (type IV collagen from human placenta, Sigma) was dissolved in 2 ml of 50 mM sodium citrate, pH 4.4. 140 mg of POROS AL 20 media (Applied Biosystems), 330 μl of 1 M sodium cyanoborohydride, and 3.45 ml of 1.5 M sodium sulfate were added, and the reaction was mixed continuously using a tube shaker at 25 °C for 16 h. The beads were washed with 50 mM sodium citrate, pH 4.4, and incubated with 6 ml of 0.1 M ethanolamine, 50 mM sodium citrate, and 330 μl of 1 M sodium cyanoborohydride, pH 4.4, at 25 °C for 2 h. The beads were further washed using H_2O Buffer and packed into a 150-μl bed volume column at 10 ml/min with H_2O Buffer. For ND samples, 20 μl of 12.7 mg/ml GST-α1I was loaded onto the collagen column following pre-equilibration with H_2O Buffer and incubated at 0 °C for 5 min. To initiate the H/D exchange reaction, 500 μl of D_2O buffer was loaded onto the column and incubated for various times (10, 100, and 1000 s at 0 °C and 300, 1000, 3000, 10,000, 30,000, and 100,000 s at 25 °C). 500 μl of 1% formic acid was applied to the column to quench the reaction and elute the GSTα1I. 150 μl of eluent was added to 12.7 μl of quench solution. Samples were stored at −80 °C prior to analysis. Incubation at 0 °C for 10, 100, or 1000 s is equivalent to incubation at 25 °C for 1, 10, or 100 s, respectively. The collagen column was regenerated between runs by washing it with 1% formic acid until the acid-eluted material measured by absorbance at 214 nm (A_{214}) reached base line, followed by equilibration of the column with neutral pH buffer (8.3 mM Tris, 150 mM NaCl, pH 7.2, with appropriate divalent cations). The efficiency of regeneration was confirmed by observation of complete restoration of ligand binding capacity assessed by both saturable binding capacity and the magnitude of material eluted after binding (measured by A_{214}). In control studies, when the acid-washed, re-equilibrated column was again eluted without protein re-loading, less than 2% of the maximum protein binding capacity of the column was eluted, demonstrating that the column had been cleared of previously bound GST-α1I by the regeneration procedure.

Calculations—DXMS Explorer was used for the data processing and reduction of hydrogen-deuterium exchange experiments. Back-exchange occurs immediately after addition of the quench solution, and corrections for it were determined by previously described methods (48) and as shown in Equation 1,

$$\text{deuteration level (\%)} = \frac{m(P) - m(N)}{m(F) - m(N)} \times 100 \quad \text{(Eq. 1)}$$

where $m(P)$, $m(N)$, and $m(F)$ are the centroid value of the partially deuterated, ND, and equilibrium deuterated peptide, respectively.

Generation of Ribbon Diagrams—The deuteration levels of peptides were further sublocalized using overlapping peptides (44). First, fragments (f_i) within each peptide were delineated in a set of overlapping peptides according to overlapping regions. At least five residues were included within each fragment to avoid overinterpreting the experimental data. Second, a variable $s_{i,t}$ was defined to represent the number of deuterium of fragment f_i values at the on-exchange time point t. Thus, a set of linear equations was established such that the sum of $s_{i,t}$ in a specific peptide was equal to the total number of deuterons observed in DXMS experiments. The best solutions were determined by linear least square fitting, with the following stipulations: (*a*) that $s_{i,t}$ is ≥0; and (*b*) for a given fragment f_i, mass shift at the longer on-exchange time point cannot be smaller than the mass shift at the shorter on-exchange time point. These fitted values were colored according to the degree of deuterium exchange (ribbon diagrams).

```
123 GSVSPTFQVV NSFAPVQECS TQLDIVIVLD GSNSIYPWES VIAFLNDLLK 170
171 RMDIGPKQTQ VGIVQYGENV THEFNLNKYS STEEVLVAAN KIVQRGGRQT 220
221 MTALGIDTAR KEAFTEARGA RRGVKKVMVI VTDGESHDNY RLKQVIQDCE 270
271 DENIQRFSIA ILGHYNRGNL STEKFVEEIK SIASEPTEKH FFNVSDELAL 320
321 VTIVKALGER IFALEALERPHRD 336
```

FIGURE 1. **Amino acid sequence of the chimeric α1I protein used in this study.** *Boxed regions* represent N- and C-terminal non-integrin sequences derived from the thrombin cleavage site and the multiple cloning site of the bacterial expression vector, respectively. Numbering is based on the full-length α1 integrin sequence and does not include the vector-derived residues. *Underlined* residues (Val-213, Gln-214, Arg-215, and Arg-218) are amino acids from the human α1I sequence that were inserted in place of the corresponding rat α1I residues (Gly-213, Arg-214, Gln-215, and Leu-218) to generate the chimeric molecule.

Generation of α1I-Collagen Model—A predicted structure of the α1I-collagen complex was created by homology modeling with the program MODELLER (55, 56). The crystal structure of the α2 I-domain in complex with collagen (Protein Data Bank code 1DZI) (6) and a structure of the α1 I domain (Protein Data Bank code 1MHP) (30) were used as templates. Type IV collagen was modeled as a trimeric THP (31). Restraints for the MIDAS site and the αC helix were taken exclusively from the α2-collagen template structure so that the modeled I domain would remain in the open conformation. The model was refined by simulated annealing under MODELLER spatial restraints from the template structures.

RESULTS

Purity and Bioactivity of α1 Integrin I Domain Proteins—The α1 I domain was expressed as a GST fusion protein comprising elements of both the rat and human α1I sequences (Fig. 1) (41). To fully characterize the properties of this chimeric form of α1I, both the GST fusion (GST-α1I) and α1I generated by cleavage of the GST tag were purified (Fig. 2*A*). Under reducing conditions, GST-α1I migrated at ~45 kDa (Fig. 2*A*, *lane 1*) and α1I migrated at ~24 kDa (*lane 2*), consistent with their predicted molecular masses (51.1 and 24.9 kDa, respectively). Using size-exclusion chromatography, α1I migrated as a monomer (apparent mass ~20 kDa), whereas GST-α1I eluted with an apparent molecular mass corresponding to a trimer (~135 kDa), consistent with the native trimeric structure of GST (57). The purified GST-α1I protein bound to type IV collagen with an EC_{50} of 31 nM (Fig. 2*B*), and this interaction could be completely blocked by incubation with AQC2 (IC_{50} = 64 pM, Fig. 2*C*). The apparent affinity of chimeric GST-α1I for collagen

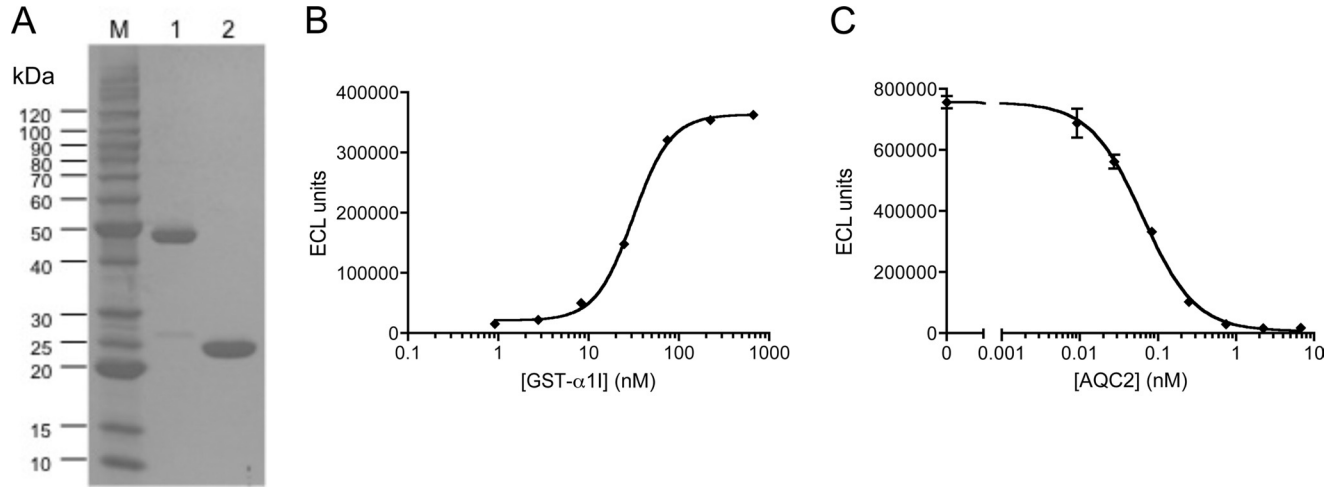

FIGURE 2. **Biochemical characterization of α1I.** *A,* purified GST-α1I (*lane 1*) and α1I (*lane 2*) were separated by 4–20% SDS-PAGE under reducing conditions and stained using Coomassie Brilliant Blue. Molecular weight markers (*M*) are shown on the *left*. *B,* binding of GST-α1I to collagen IV was measured using an electrochemiluminescence assay (EC_{50} = 31 nM). *C,* inhibition of GST-α1I/collagen IV binding by antibody AQC2 was measured using the electrochemiluminescence assay (IC_{50} = 64 pM).

was identical to what we have observed using the corresponding rat GST-α1I (data not shown), and is consistent with previously reported affinities for the human GST-α1I/collagen IV interaction (58, 59). The chimeric GST-α1I was utilized for these studies because the corresponding human protein was poorly soluble under the physiological conditions used to assess its biochemical and functional attributes.

Effect of Divalent Cations on the Stability of α1I—All integrins require divalent cations for ligand binding. A previous study, using circular dichroism, demonstrated the stabilizing effect of divalent cations (Mg^{2+} and Mn^{2+}) on α1I (41). We have extended these observations using differential scanning calorimetry (DSC) (Fig. 3). The measured melting temperature (T_m) for α1I in the presence of the chelating agent EDTA was 57.9 °C. A single cooperative unfolding transition was observed (Fig. 3*A*). No significant change occurred in the presence of 10 mM $CaCl_2$ alone (T_m = 58.5 °C) or in 1 mM $CaCl_2$, 1 mM $MgCl_2$, which approximates physiological cation concentrations (T_m = 58.2 °C, Fig. 3*A*). Addition of 10 mM Mg^{2+} (T_m = 61.4 °C) or 10 mM Mn^{2+} (T_m = 62.0 °C) alone increased the thermal stability of α1I significantly. The effects of Mn^{2+} and Mg^{2+} were concentration-dependent, as determined in a second set of experiments showing stabilizations of as much as 8–10 °C (Fig. 3*B*). The EC_{50} values for Mn^{2+} and Mg^{2+} were 0.16 and 1.8 mM, respectively. These values agree with Mn^{2+} and Mg^{2+} concentrations previously shown to support collagen binding to α1β1 (42, 60). Similar results were obtained using the GST fusion protein (GST-α1I), although under some conditions the I domain transition was masked by the GST unfolding transition at ~57–59 °C (data not shown). To complement the thermal stability measurements, the impact of Mn^{2+} on susceptibility of α1I to the denaturant urea was measured by monitoring intrinsic tryptophan fluorescence (Fig. 3*D*). α1I has a single tryptophan residue (Trp-158), located near the MIDAS site. In the absence of divalent cation, ~5 M urea was required for 50% denaturation, and Mn^{2+} significantly increased the stability of α1I domain, to an EC_{50} of ~7 M urea.

Ca^{2+} does not support α1β1 collagen binding, and it has been shown to bind with poor (mM) affinity to integrin I domains (61–63). Unlike Mn^{2+} and Mg^{2+}, Ca^{2+} did not stabilize α1I toward thermal denaturation at concentrations up to 100 mM (Fig. 3*B*). However, at equimolar concentrations (10 mM), Ca^{2+} completely reversed the stabilizing effect of Mg^{2+}, indicating that Ca^{2+} is capable of binding to α1I and displacing Mg^{2+} from the MIDAS site. Interestingly, in urea denaturation studies, addition of 10 mM Ca^{2+} increased the urea concentration required for half-maximal denaturation to ~7 M, similar to the amount of stabilization observed with Mn^{2+} (Fig. 3*D*). Similar results were observed with urea denaturation studies using the rat α1 I domain (Ref. 41 and data not shown). These results clearly indicate that Ca^{2+} is capable of binding to the α1I MIDAS, even though it does not effectively support collagen ligand binding. The difference between the thermal and chemical denaturation results suggests that Ca^{2+} binding affects the local environment around the MIDAS such that it can be detected by chemically induced unfolding but not by calorimetry, which is a more global measure of stability.

DXMS of α1I—DXMS was utilized to evaluate the structural properties of unliganded α1I in solution and to provide a reference for subsequent experiments incorporating bound ligands. The DXMS method measures the solvent accessibility of main-chain amides in defined segments of a protein through a combination of time-dependent deuterium exchange, limited proteolysis, and mass spectrometry (33–40). Percent deuteration is operationally defined as the number of deuterium ions incorporated into a given peptide at a fixed time, divided by the maximum level incorporated at equilibrium. The DXMS profile of α1I in the presence of 10 mM $MgCl_2$ is shown in Fig. 4. Briefly, a sample of α1I was diluted 1:3 into a deuterated buffer and incubated at 25 °C for defined time intervals from 1 to 1000 s. The exchange reaction was quenched by lowering the temperature and pH, and samples were digested with pepsin and analyzed using LC-MS. The sequence coverage of α1I was 93%. The data generated from 77 overlapping peptides was used to gen-

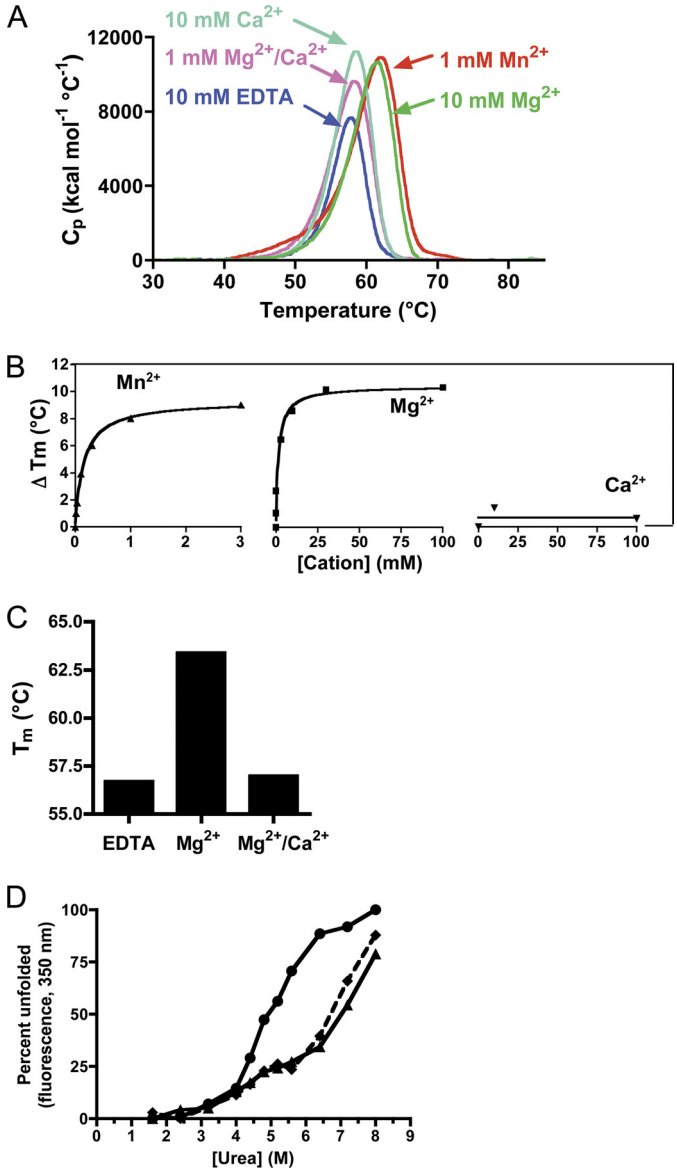

FIGURE 3. **Metal ion-mediated stabilization of α1 I domain.** *A,* thermal denaturation curves. Purified α1I was incubated for 1 h with either 10 mM EDTA (*blue*), 10 mM $CaCl_2$ (*light green*), 1 mM $MgCl_2$ + 1 mM $CaCl_2$ (*pink*), 10 mM $MgCl_2$ (*dark green*), or 1 mM $MnCl_2$ (*red*) and analyzed using DSC. *B,* effect of varying concentrations of $MnCl_2$, $MgCl_2$, or $CaCl_2$ on the melting temperature (T_m, in °C) of α1I measured by DSC. The results were plotted as change in T_m (ΔT_m) relative to a reference sample containing 10 mM EDTA. *C,* reversal of Mg^{2+}-induced stabilization of α1I by Ca^{2+}, as measured by DSC. The T_m values for samples of α1I in the presence of 10 mM EDTA, 10 mM $MgCl_2$, or 10 mM $MgCl_2$ + 10 mM $CaCl_2$ were determined using DSC. *D,* effect of metal ions on the chemical denaturation of α1I. Purified α1I in buffer containing 10 mM EDTA (*circles*), 1 mM $MnCl_2$ (*triangles*), or 10 mM $CaCl_2$ (*diamonds*) was incubated with urea at the indicated concentrations, and the fraction of unfolded protein was determined by monitoring tryptophan fluorescence (excitation 280 nm and emission 350 nm). Representative data confirmed by three independent experiments are shown.

erate a one-dimensional ribbon map representing the average deuterium incorporation throughout the protein sequence (Fig. 4*A*). This linear map was annotated with the secondary structural elements identified from the α1I crystal structure (Fig. 4*B*). This experiment revealed several regions of α1I with very high incorporation of deuterium even at short incubation times, indicative of a highly flexible and dynamic structure. For example, N-terminal residues 134–143 appeared largely unfolded, exchanging >80% of the accessible amide protons within 1 s in D_2O. This is consistent with the lack of any observed density N-terminal to residues 141–143 in α1 I domain crystal structures 1QC5 (28), 1PT6 (27), and 1CK4 (26). Similarly, residues at the C terminus (residues 333–336) were also exchanged very rapidly, consistent with the crystallographically determined terminus of the C-terminal α7 helix at position 332 (26). A third region comprising residues 291–295, a loop that connects the αC and α6 helices, also exchanged rapidly. As discussed below, the αC helix and adjacent residues play a key role in collagen binding and selectivity by this integrin. The αC helix itself (residues 283–287) exchanged more slowly than these other regions, but it still showed >75% deuterium incorporation within 300 s. The remainder of the α1I sequence, including the α-helical and β-strand regions forming the classic dinucleotide-binding fold, exchanged much more slowly, with most showing <50% deuterium incorporation even with longer D_2O incubation times. The exchange data at 100 s were overlaid on the three-dimensional structure of α1I (Fig. 4*C*). From this overlay it is clear that the slowest exchanging regions are within well defined secondary structural elements (*e.g.* the α3 and α5 helices, and the βE strand), although the faster exchanging regions are contained within or at the interfaces with less structured loops. The DXMS profile of the GSTα1I fusion protein was also determined (Fig. 4*A*) and was very similar to the untagged α1I.

Effect of Divalent Cations on α1I Domain Solution Structure—We next evaluated the impact of MIDAS site occupancy with different divalent cations on the DXMS exchange properties of α1I. The incorporation of deuterium into α1I was assessed in the presence of 5 mM EDTA (apo-α1I) or in 10 mM Mg^{2+}, 0.5 mM Mn^{2+}, or 1 mM Ca^{2+} (Fig. 5). Relative to apo-α1I, all three cations significantly decreased the exchange rates in multiple peptides, including residues 157–171, 195–206, and 250–264, as shown in Fig. 5*A*. No regions showed increased exchange rates in the presence of cation, suggesting an overall decrease in flexibility throughout the α1I structure. Difference maps comparing each of the cation-bound states *versus* apo-α1I (Fig. 5*B*) show that, at 100 s, slower exchange rates were observed over the majority of the α1I sequence. Larger decreases in exchange rates were observed with Mg^{2+} and Mn^{2+}, consistent with the stabilizing effects measured using DSC and tryptophan fluorescence. Ca^{2+} led to smaller but still significant effects on exchange rates, further demonstrating that Ca^{2+} is competent to bind the MIDAS site and partially stabilize α1I.

Generally, the exchange rates of α1I in Mg^{2+} and Mn^{2+} were very similar (Fig. 5). This was confirmed by generating difference maps comparing these two conditions over a wide range of exchange times (1–300 s) (Fig. 6*A*). One set of peptides covering the αC helix region, however, exchanged much faster in Mn^{2+} than in Mg^{2+}. This was exemplified by the 283–290-residue peptide, which incorporated notably higher levels of deuterium at exchange times <100 s in the presence of $MnCl_2$ than it did in $MgCl_2$ (Fig. 6*B*). This result was observed even when the protein was first treated with EDTA and reconstituted with excess $MgCl_2$ or $MnCl_2$, indicating that the result was not due to the effect of metals introduced during protein production or purification (data not shown). The observed differences in

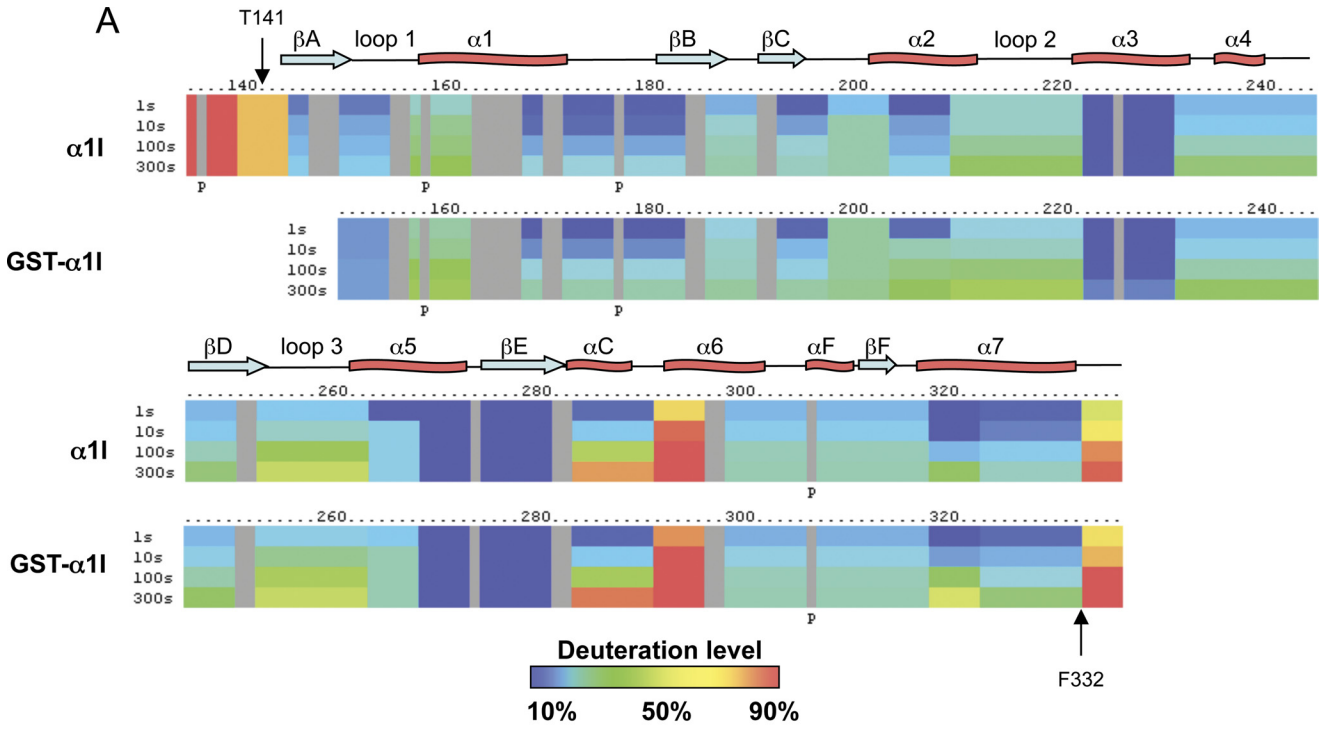

B

Feature	Position
βA	Leu143–Asp150
α1	Pro157–Lys170
βB	Gln180–Tyr186
βC	Val190–Phe194
α2	Ser201–Lys211
α3	Met221–Glu232
α4	Thr235–Gly239
βD	Lys245–Thr252
α5	Arg261–Glu272
βE	Ile274–Ile281
αC	Gly283–Arg287
α6	Thr292–Ser301
αF	Pro306–His310
βF	Phe311–Val314
α7	Glu317–Phe332

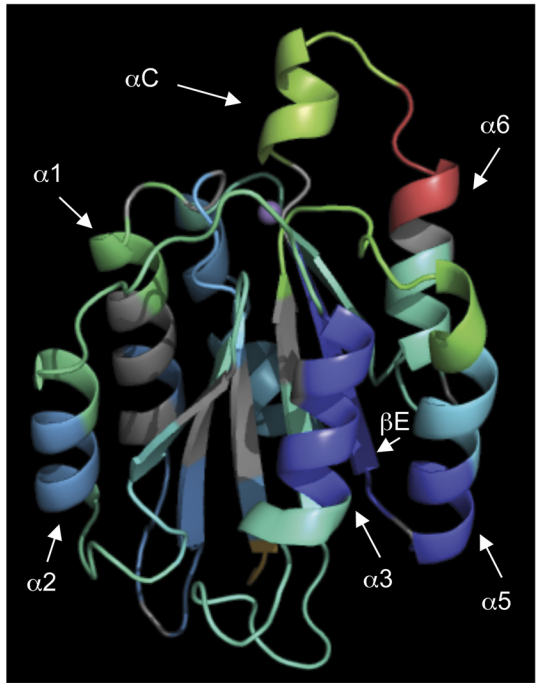

FIGURE 4. **Deuterium ion incorporation into α1I in the presence of 10 mM $MgCl_2$.** *A*, one-dimensional ribbon map. The H/D exchange profiles of α1I and GST-α1I are shown. The numbers *above* the map represent the primary sequence (residues 134–336 of α1I or 149–336 of GSTα1I, numbered as in Fig. 1), and the positions of I domain structural elements are annotated above (*red twist*, α-helix; *blue arrow*, β-strand). Each *bar below* the sequence is divided into rows corresponding to each time point from 1 to 300 s (top to bottom). Color coding indicates the percentage of deuterium incorporation into exchangeable amide protons after a given incubation time. *Vertical arrows* indicate residues Thr-141 and Phe-332, which are the N- and C-terminal residues, respectively, within which the α1 I domain crystal structure (Protein Data Bank code 1CK4) showed measurable electron density. *P* indicates the positions of proline residues, which have no exchangeable protons. Other areas in *gray* did not have sufficient coverage in the map to allow accurate quantitation of deuteration levels. *B*, annotated list of the primary structural features of α1I and the corresponding positions within the sequence (26). *C*, exchange rates at 100 s were mapped onto α1I crystal structure 1MHP. Color coding indicates the percentage of deuterium incorporation into exchangeable amide protons (identical scale as in *A*). The positions of prominent structural elements are indicated, and the metal ion in the MIDAS is represented by a *gray sphere*.

exchange rates in this region were surprising, because Mg^{2+} and Mn^{2+} were shown to bind integrin I domains with similar geometries (11, 62, 64) and showed essentially identical abilities, at saturating concentrations, to stabilize integrin structure (Fig. 3) and promote ligand binding (42, 60). The faster exchange rate in the presence of Mn^{2+} has led us to generate a new model to explain the differences in the relative abilities of various metal ions to activate integrin I domains, in which

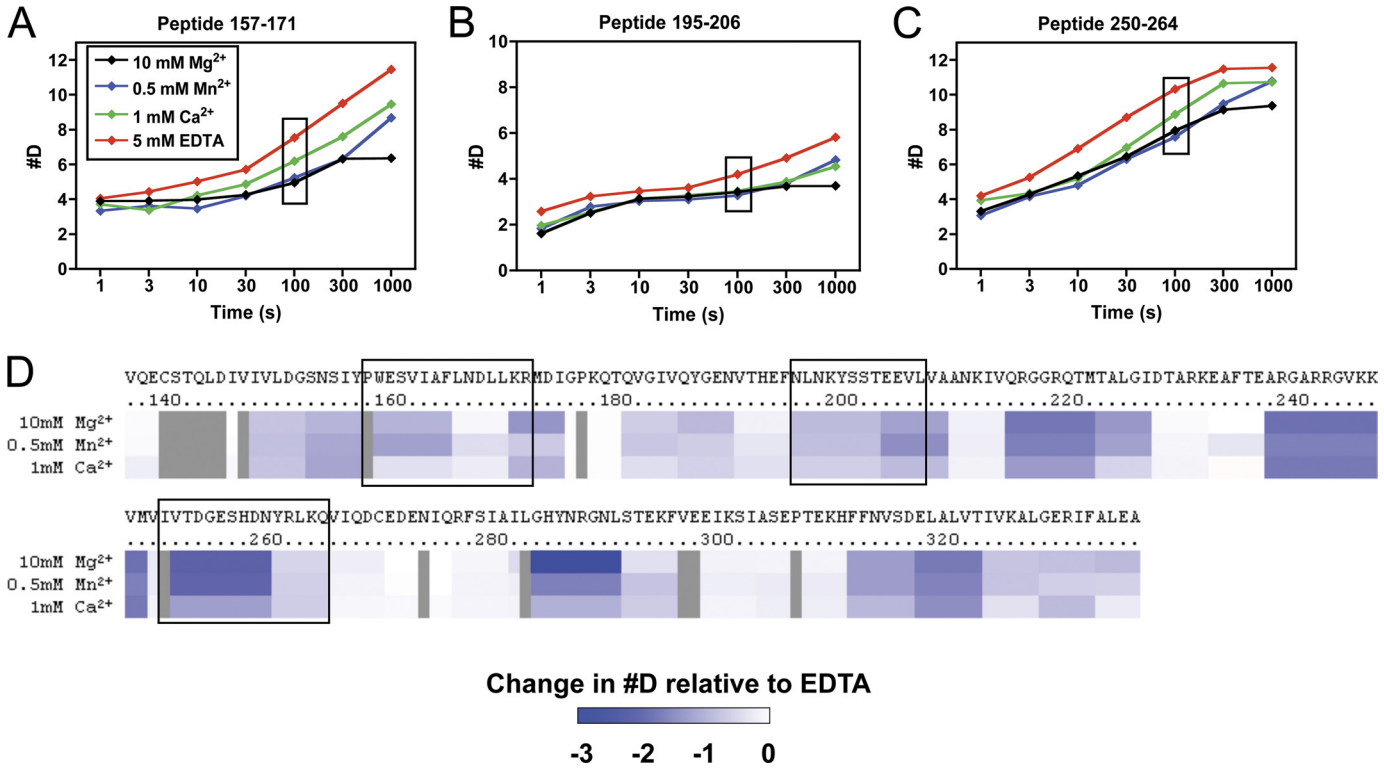

FIGURE 5. **Divalent cations decrease the rate of H/D exchange in α1I.** *A–C,* time courses of deuterium incorporation into peptides 157–171, 195–206, and 250–264, in the presence of 10 mM $MgCl_2$, 0.5 mM $MnCl_2$, 1 mM $CaCl_2$, or 5 mM EDTA. Data are plotted as the number of deuterium ions (*#D*) incorporated into each peptide at a given time. *D,* difference map, indicating the change in *#D* in the presence of each metal ion relative to EDTA, after 100 s of incubation. The peptides described in *A–C* are indicated with *boxes*. The threshold for this plot was defined to resolve changes of up to ±3 deuterium ions/peptide.

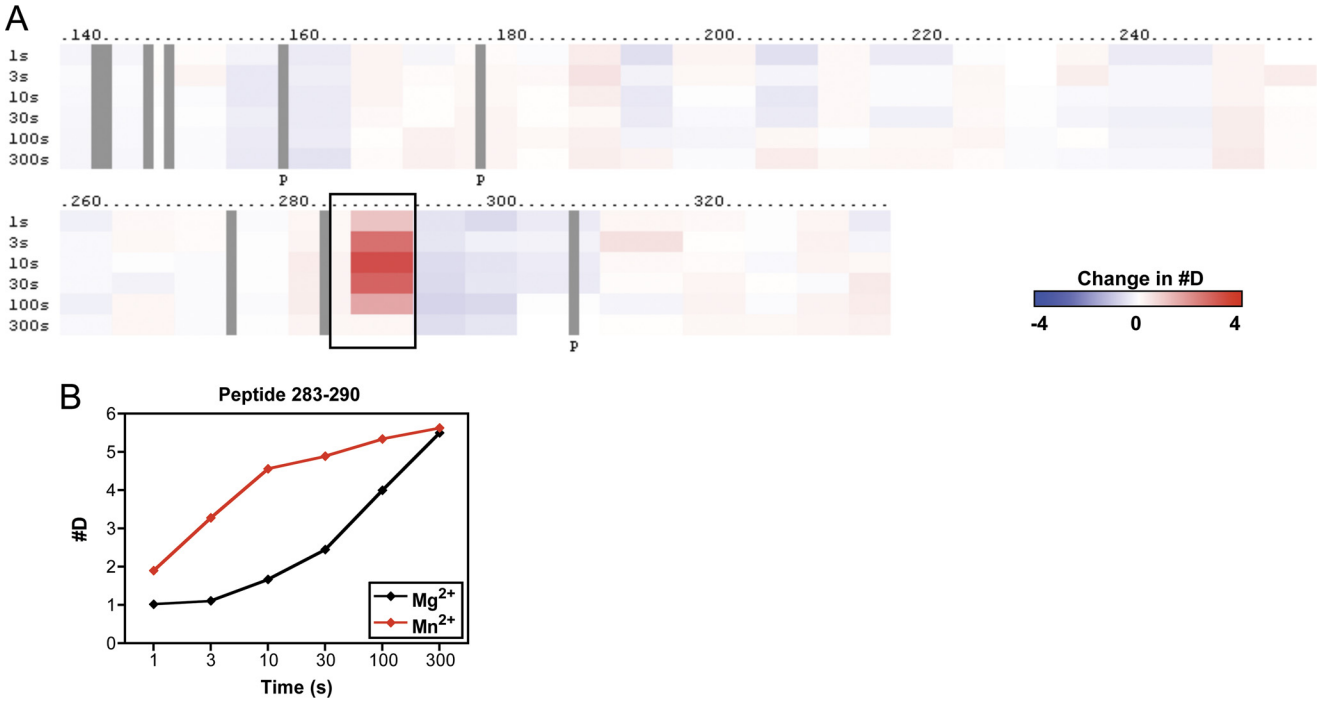

FIGURE 6. **Mg^{2+} and Mn^{2+} induce different structures in the αC helix.** *A,* difference map depicting deuterium ion incorporation into α1I in the presence of 0.5 mM $MnCl_2$ or 10 mM $MgCl_2$. The number of deuterium ions (*#D*) incorporated into each peptide at a given time was determined, and the value of *#D* in Mg^{2+} was subtracted from that in Mn^{2+}. The threshold for this plot was defined to resolve changes of up to ±4 deuterium ions/peptide. Residues 283–290, corresponding to one of the peptides that exchanged notably faster in Mn^{2+} than in Mg^{2+}, are indicated by a *box*. *B,* representative deuterium buildup curve for peptide 283–290 in the αC helix.

Mn^{2+} preferentially unfolds the αC helix by assuming a penta-coordinated geometry (discussed below). In any case, the ability of Mn^{2+} and Mg^{2+} to induce detectably different conformational changes in α1I indicates that, unlike previous suggestions (65), the choice of divalent cation impacts the local structure around the ligand-binding site.

DXMS Profile of the Complex between α1I and Full-length Collagen—A crystal structure of α2I in complex with a triple-helical collagen-based peptide, but not a corresponding α1I-collagen peptide structure, has been reported (6). Because intact fibrillar collagen cannot be crystallized, no structure has been reported for full-length collagen bound to an integrin. To explore the nature of these interactions under native conditions, we determined the DXMS exchange pattern of the α1I protein bound to full-length type IV collagen. For these studies, a complex was formed by incubating the GST-α1I fusion protein with collagen IV that was immobilized on a bead-based support in the presence of 10 mM $MgCl_2$. Deuterium exchange was then performed on the immobilized GST-α1I. The DXMS exchange rates in the presence of collagen were subtracted from those determined for GST-α1I alone to generate a series of difference maps (Fig. 7*A*). The exchange data at early (1 s) and late (10,000 s) time points were superimposed on a model of α1I bound to collagen IV (Fig. 7*B*), generated by docking α1I, in an open conformation, with a collagen THP as described previously (31).

Regions at the interface of protein-protein binding surfaces are typically protected from amide exchange with water (66). Using DXMS, only residues in MIDAS loop 2 of α1I, exemplified by peptide 207–221, showed significant protection against deuterium exchange when bound to collagen (Fig. 7*A*). The structure of the α2I-collagen peptide complex suggested interactions between all three MIDAS loops (151–156, 212–220, and 253–260) and the collagen peptide (6). Similar interactions were proposed for the α1I-collagen IV structure, including stabilizing interactions with collagen involving Arg-218 in loop 2 and Glu-255 in loop 3 (31). The DXMS results indicate that little change in solvent accessibility occurs in either loop 1 or loop 3 upon binding to collagen. A closer examination of the model (Fig. 7*B*) suggested an explanation for this result. Loops 1 and 2 both make significant contacts with the collagen. Loop 2 has exposed backbone amides, particularly in residues 215–219, which are apparently protected upon collagen binding. Contacts of loop 1 with collagen are mediated mainly by the side chains of Asn-153 and Tyr-156, but the backbone amides of loop 1 are largely buried by folding within α1I itself. As a result, exchange is substantially slower in loop 1 even in the absence of collagen (see Fig. 4). Consequently, it is not surprising that collagen binding has a negligible effect on the loop 1 amides. In contrast, loop 3 has exposed backbone amides, but the model suggests it has very limited contact with collagen, which explains the limited protection observed in loop 3. This result does not support the proposal that Glu-255 forms a salt bridge with collagen (31) but is instead consistent with data showing that the corresponding glutamic acid in α2 (Glu-256) is not critical for ligand binding (67).

Several regions of α1I displayed significantly increased rates of exchange when complexed with collagen (Fig. 7). These increased rates of exchange reflect greater solvent exposure of the affected amide protons and suggest an increase in flexibility in these regions. The changes were clustered in the C-terminal region of the molecule. Residues 283–290, which include the αC helix, displayed very rapid exchange, with essentially complete deuterium incorporation within 1 s of solvent exposure, suggestive of extensive structural changes in this region. Residues 318–332, in the C-terminal α7 helix, and other intervening structural elements between αC and α7 (residues 298–317) also showed notable increases in the rates of deuterium incorporation, although exchange was not as fast as in the αC helix. These results provide direct evidence that α1I undergoes an allosteric conformational change in the C-terminal helix upon ligand binding, as has been postulated for other I domain-containing integrins on the basis of static crystal structures (3, 4, 6, 12), In addition, the striking increase in conformational flexibility of the α7 helix in the presence of ligand provides direct support for the proposal that the I domain C-terminal helix is unusually mobile (5), although this mobility appears to be induced by ligand binding rather than an intrinsic property of the unliganded I domain structure (discussed below).

Effect of the "Pseudo-ligand Mimetic" Antibody AQC2 on α1I Exchange Rates—The α1 I domain was previously crystallized with a Fab fragment of the anti-α1β1 function-blocking antibody AQC2 (30). AQC2 can be classified as a pseudo-ligand mimetic antibody, because it binds to α1I in a ligand-mimetic fashion via direct interaction of an antibody aspartate residue with the MIDAS metal ion, but it does not induce a change to the open conformation (30, 68). The AQC2-α1I complex was generated in the presence of Mg^{2+}, and DXMS studies were carried out in a similar manner as described above for the collagen-α1I complex (Fig. 8). A difference map is shown in Fig. 8*A*, with blue and red regions indicating decreased and increased exchange, respectively, upon antibody binding. The data at 1 and 1000 s were mapped onto the co-crystal structure of the AQC2-α1I complex (Fig. 8*B*) (30).

The most dramatic decreases in exchange rates were in residues 214–226, corresponding to MIDAS loop 2. This is consistent with the inability of AQC2 to bind to wild-type rat α1I (41), which has four amino acid differences in the 213–218-residue region, and with direct evidence from the crystal structure showing Arg-218 located inside of a cleft within the antibody (30). As in the collagen-α1I complex, no significant effects on MIDAS loops 1 or 3 were observed. The correlation between the collagen-α1I and AQC2-α1I exchange patterns within the MIDAS region indicates that the local interactions of AQC2 with α1I at the MIDAS site are very similar to those of the native ligand. This result is in striking contrast to the crystal structure of AQC2-α1I, which showed interactions of the antibody with all three loops, and suggests that the loop 2 region of α1I is predominantly responsible for the interaction of α1I with the antibody.

Similar to the collagen complex, the exchange rate in the αC helix (residues 283–290) increased upon AQC2 binding, indicating that the antibody induces a significant loss of secondary structure in this region. However, unlike collagen binding, the structural changes in the α7 C-terminal helix (residues 318–332) were modest. The crystal structure of α1I bound to AQC2

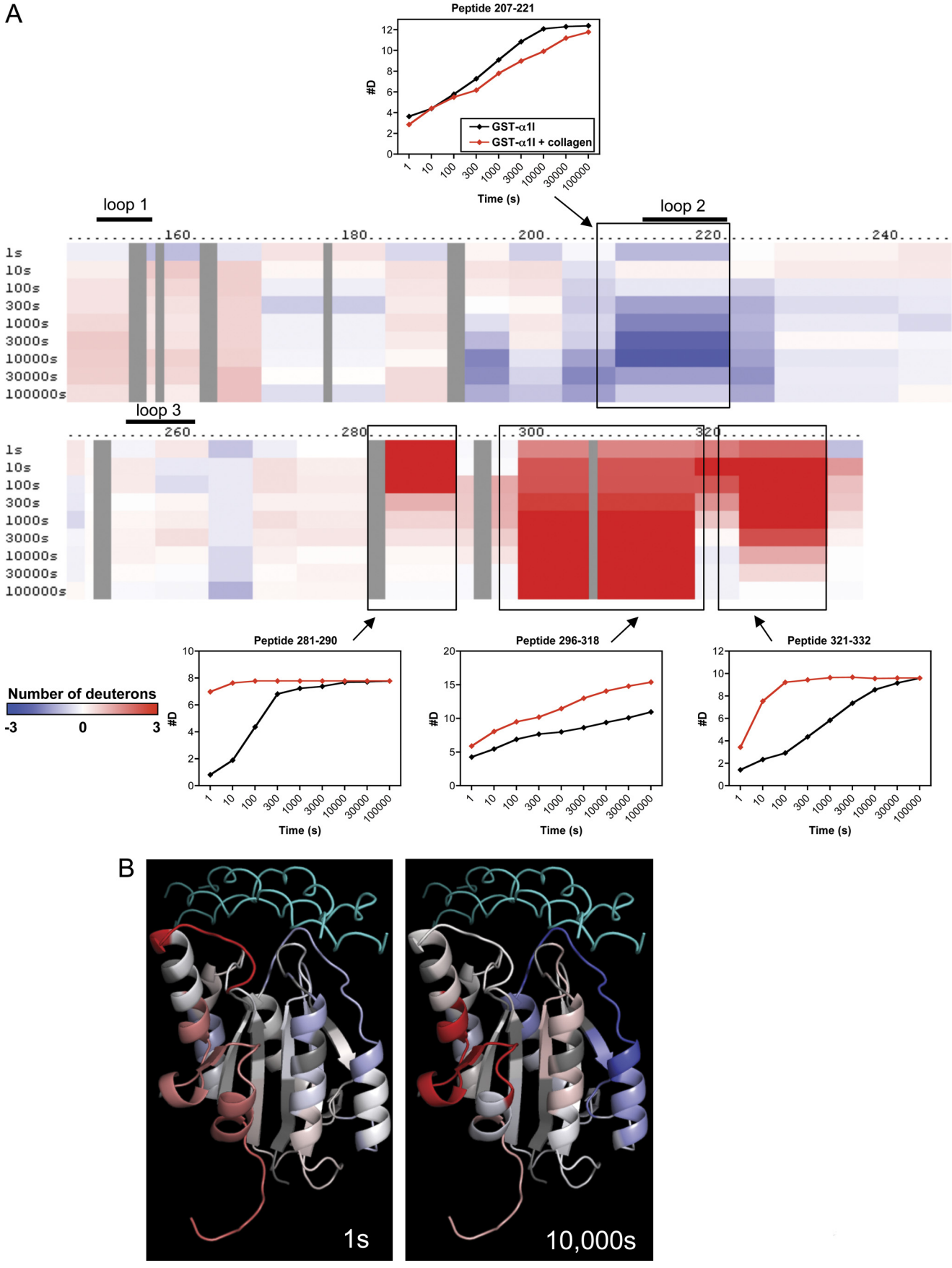
A
Peptide 207-221
#D
Time (s)
GST-α1I
GST-α1I + collagen
loop 1
loop 2
loop 3
1s
10s
100s
300s
1000s
3000s
10000s
30000s
100000s
Number of deuterons
-3
0
3
Peptide 281-290
Peptide 296-318
Peptide 321-332
B
1s
10,000s

(30) adopted a closed conformation very similar to that of the unbound α1I (26, 28), with no evidence for a shift in the C-terminal helix. Thus, even though AQC2 binding to α1I leads to similar effects as the native ligand within the local region surrounding the MIDAS, it does not induce allosteric changes that would indicate a shift from the closed to the open conformation, characteristic of ligand binding.

DISCUSSION

We have successfully used hydrogen-deuterium exchange mass spectrometry (DXMS) to explore the conformational dynamics of cation, ligand, and antibody binding to the I domain of integrin α1 in aqueous solution. Most detailed structural information on integrin I domains is based on crystallographic data, so DXMS provided a unique opportunity to study the solution dynamics of the α1 I domain. The DXMS mapping method provided coverage of 93% of the α1I sequence with over 200 exchangeable hydrogens. The average peptide length was 15 amino acids. The observed H/D exchange rates for unliganded α1I were remarkably consistent with the structural elements observed in crystallographic studies of this domain. Regions at the N and C termini of the protein that did not show measurable density in the crystal structures incorporated deuterium rapidly, establishing the limits of the globular domain as comprising residues Asp-144 to Phe-332. Slow exchanging regions throughout the sequence largely correlated with defined secondary structural elements, although the unstructured loop regions, including the MIDAS loops involved in ligand binding, exchanged more rapidly.

In I domain-containing integrins, the I domain MIDAS coordinates a divalent cation such as Mg^{2+}, which interacts directly with an acidic residue (Asp or Glu) in the ligand. Some nonphysiological cations, such as Mn^{2+}, are capable of activating integrins much more strongly than Mg^{2+}, whereas Ca^{2+} is incapable of mediating ligand binding, but the structural basis for this phenomenon is not well understood. Previous studies established that Mg^{2+} and Mn^{2+} at millimolar concentrations stabilize the I domain from α1 (41). Using DSC, we observed up to 8–10 °C increases in the T_m values for α1I at saturating concentrations of either Mn^{2+} or Mg^{2+}. This overall stabilization by Mn^{2+} or Mg^{2+} was further established using DXMS, which revealed decreased H/D exchange rates throughout the α1I sequence in the presence of these cations.

Interpretation of the role of Ca^{2+} in integrin/ligand interactions is complicated (69). In α I domains, Ca^{2+} affinity for MIDAS, and its ability to regulate ligand binding, is both concentration- and activation-state dependent (61, 70, 71). The affinity of the αM I domain for Ca^{2+} was shown to be low (millimolar) (61–63), and quantum calculations on the αL I domain predicted that the Ca^{2+}-bound state would have lower affinity than either the Mg^{2+}- or Mn^{2+}-bound state for ligand (71). However, some integrin I domains have shown differences in their relative abilities to bind calcium (70, 72), suggesting that the affinity of each I domain MIDAS site for Ca^{2+} may be different. Interestingly, even though we observed no effect of millimolar levels of Ca^{2+} by DSC, several other measures provided clear evidence for a stabilizing effect of Ca^{2+} on α1I. DXMS showed decreases in exchange rates throughout the α1I sequence. The concentration of urea required to denature α1I was increased by 2 M in the presence of 10 mM Ca^{2+}, which was comparable in magnitude to the effect of Mn^{2+}. Finally, Ca^{2+} at an equimolar concentration reversed the stabilizing effect of 10 mM Mg^{2+} ions. Thus, our results demonstrate that Ca^{2+} is capable of binding to the α1I MIDAS and that even though Ca^{2+} binding does not stabilize the I domain to thermal denaturation or support ligand binding, it significantly impacts the solution dynamics of the protein.

The DXMS patterns of α1I in Mg^{2+}, Ca^{2+}, and Mn^{2+} were very similar, except for a striking difference in the αC helix, a structural element unique to collagen-binding integrins that is believed to be critical for binding and collagen subtype selectivity (6, 59, 73). Relative to apo-α1I, saturating concentrations of Mg^{2+} stabilized the αC helix toward deuterium exchange to a much greater extent than either Mn^{2+} or Ca^{2+}. This result was surprising, because both Mg^{2+} and Mn^{2+} support binding of collagen IV to α1β1 at these concentrations (42, 58), and crystallographic data on integrin I domains support the concept that Mg^{2+}- and Mn^{2+}-bound I domains form essentially identical structures (65). These data, in conjunction with the recently reported crystal structure of α1I with the activating mutation E317A (32), led us to propose a model for collagen-binding integrin I domain activation that provides a structural basis for the enhanced activating ability of Mn^{2+} and the inability of Ca^{2+} to mediate ligand binding (Fig. 9). The α1I(E317A) structure, which was the first to display an unwound αC helix in an I domain in the absence of a bound collagen peptide, contained a unique penta-coordinated Mg^{2+} in the MIDAS, suggesting that a change from penta- to hexa-coordinated metal ion upon ligand binding drives allosteric conformational changes within α1I. In our model, the closed conformation, with a hexa-coordinate metal ion and tightly wound αC helix, is in equilibrium with the activated conformation, containing a penta-coordinate metal and unwound αC helix. Collagen ligand binding leads to conversion back to the more stable hexa-coordinate geometry and induces allosteric changes in the C-terminal helices. Importantly, Mg^{2+} ions pay a significant energetic penalty for deviating from a hexacoordinate (octahedral) geometry, whereas Mn^{2+} is capable of adopting lower coordination states (32). Thus, Mn^{2+}, with a lower energetic barrier to adopting the activated conformation, is more effective at driving the opening of the αC helix and enabling ligand binding. Ca^{2+}, which is unable to adopt a pentavalent conformation, is incapable of mediating ligand binding.

FIGURE 7. **Effect of collagen binding on GST-α1I domain hydrogen-deuterium exchange rates.** *A*, difference map indicating exchange rates in free *versus* collagen-bound GST-α1I in the presence of 10 mM $MgCl_2$. *Blue regions* indicate decreased exchange (*#D*), and *red regions* indicate increased exchange, in the presence of collagen. The threshold for this plot was defined to resolve changes of up to ±3 deuterium ions/peptide. Exchange curves for representative peptides 207–221, 281–290, 296–318, and 321–332 are shown and indicated with *boxes* on the map. *B*, exchange rate differences at 1 and 10,000 s were mapped onto a model of the α1I-collagen complex. The THP used to generate the model is shown in *cyan* (at *top* of figure). Color coding on α1I is identical to that shown in *A*.

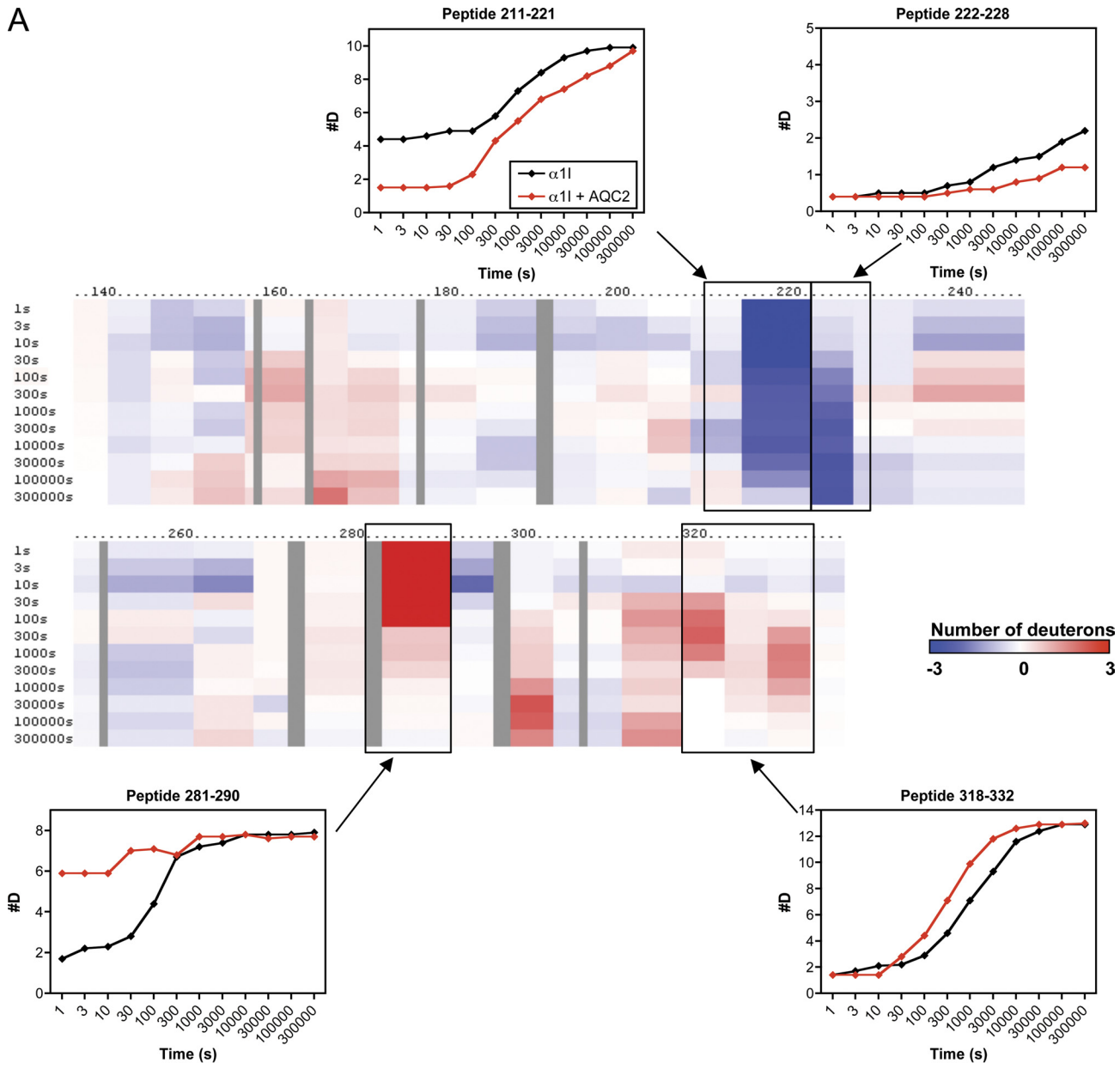
A
Peptide 211-221
#D
Time (s)
α1I
α1I + AQC2
Peptide 222-228
#D
Time (s)
1s
3s
10s
30s
100s
300s
1000s
3000s
10000s
30000s
100000s
300000s
Number of deuterons
-3
0
3
Peptide 281-290
#D
Time (s)
Peptide 318-332
#D
Time (s)

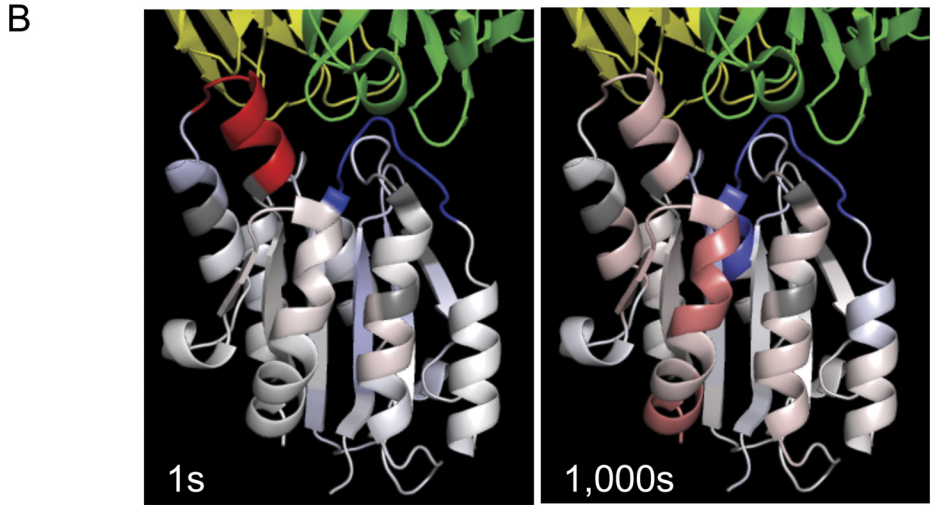
B
1s
1,000s

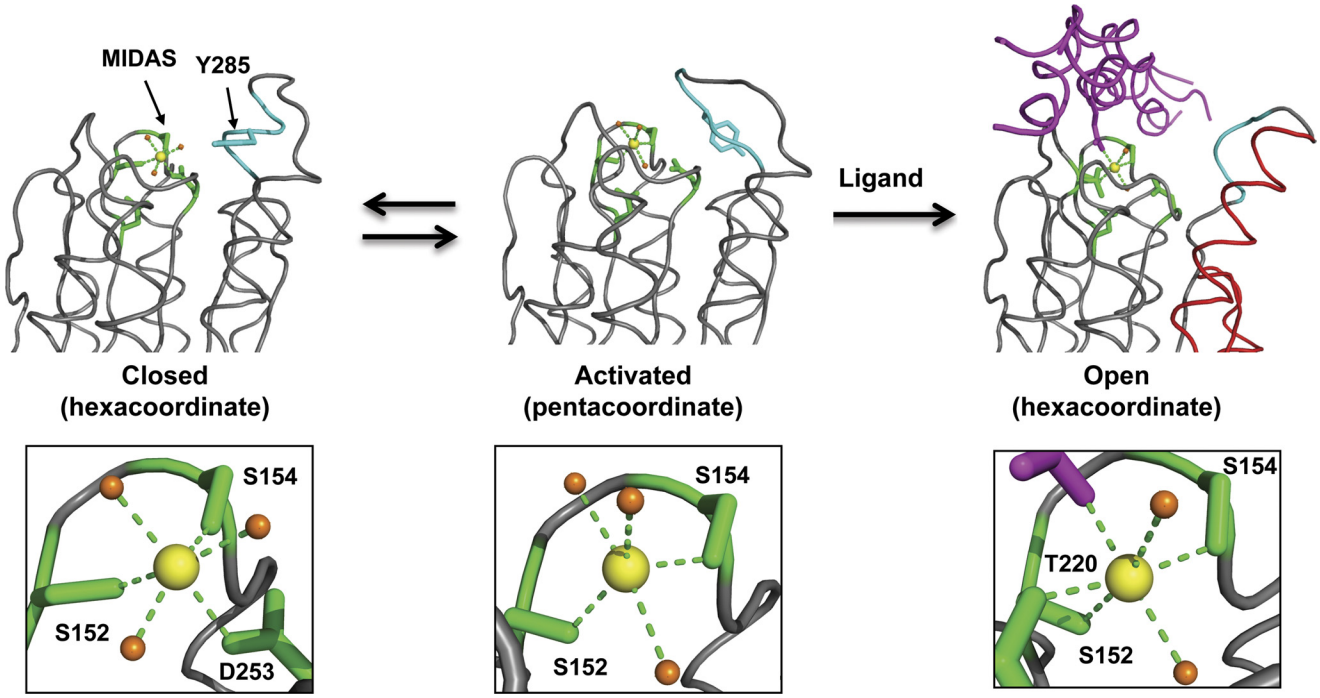

FIGURE 9. **Model for collagen-binding integrin I domain activation.** Structures of closed, activated, and open I domains were modeled based on Protein Data Bank entries 1QC5 (α1I), 4A0Q (α1I (E317A)), and 1DZI (α2I-THP complex). The MIDAS site (*green*) and αC helix (*cyan*) are *highlighted*, and the C-terminal α6 and α7 helices (*red*) and bound collagen (*magenta*) are indicated in the open structure. The side chain of Tyr-285 is shown for orientation in the closed and activated α1 conformations. *Insets* show the coordination states of the metal ion (*yellow*). Bound water molecules are shown in *orange*.

The observation of such striking metal ion-mediated differences in the αC helix conformation demonstrates the importance of studying the dynamics of integrins in solution as a complement to crystallographic studies. Because there are no crystal structures of free (not bound to ligand or antibody) α1 or α2 I domains in Mn^{2+}, we cannot rule out the possibility that Mg^{2+} and Mn^{2+} would produce different conformations of αC even in a crystalline state. More likely, however, this difference is only detectable in solution, where crystal packing effects are eliminated. The concept that Mg^{2+} and Mn^{2+} induce different conformations of αC in solution is supported by tryptophan fluorescence studies on α1I, which demonstrated that binding of Mg^{2+} led to conformational changes in the vicinity of Trp-158, which is located at the end of MIDAS loop 1, very near the αC helix in the three-dimensional structure of α1I, and that these changes differed from the effects of added Mn^{2+} (72).

DXMS provided an ideal tool to characterize the conformational changes in α1I induced upon collagen binding and to test the existing models for integrin I domain/ligand interactions. The DXMS pattern of α1I bound to collagen showed significantly reduced exchange only in MIDAS loop 2, suggesting that this region of α1 integrin is a critical element mediating the interaction with collagen. Collagen also induced faster exchange in the αC, α6, and α7 helices, consistent with models in which ligand binding causes a downward shift of the C-terminal α7 helix of the I domain, leading to engagement of Glu-335 (in the case of α1 integrin) with the MIDAS site of the β subunit I-like domain (1). It has been proposed that the α7 helix is intrinsically mobile, allowing it to trigger this process with minimal energetic penalty (5, 10). Our DXMS data on α1I indicate that the flexibility of α7 is greatly increased upon ligand binding. We therefore propose a modification to this model in which ligand binding is responsible for relaxing the α7 helical structure and facilitating the conformational changes necessary for effective intersubunit communication, *e.g.* in outside-in signaling.

One of the key differences between the studies reported here and those previously described is the use of full-length collagen instead of a THP fragment. Solution binding studies on α2 I domain binding to a collagen THP have been reported using NMR (74). A number of residues located near the α7 helix showed changes in chemical shift pattern, although only one residue (Gly-329, equivalent to Gly-328 in α1I) within α7 itself was noted. The relatively small number of chemical shift changes observed in this region compared with our observations using DXMS on α1I-collagen could be due to limitations of the NMR method, such as the inherently reduced peak intensity observed upon peptide binding. Alternatively, the use of a THP instead of a full-length collagen ligand may have led to less robust conformational changes in the integrin. It is important to note that a single molecule of collagen contains multiple integrin-binding sites with differing affinities (75). This has the

FIGURE 8. **DXMS exchange rates for α1I bound to antibody AQC2 in the presence of 1 mM $MgCl_2$.** *A*, difference map indicating exchange rates in free *versus* AQC2-bound α1I. *Blue regions* indicate decreased exchange (*#D*), and *red regions* indicate increased exchange, in the presence of antibody. The threshold for this plot was defined to resolve changes of up to ±3 deuterium ions/peptide. Exchange curves for representative peptides 211–221, 222–228, 281–290, and 318–332 are shown and indicated with *boxes* on the map. *B*, exchange rate differences at 1 and 1000 s were mapped onto the crystal structure of the AQC2-α1I complex. Antibody heavy and light chains are shown in *green* and *yellow*, respectively. Color coding on α1I is identical to that shown in *A*.

potential to lead to dispersion in the DXMS signal. It is unclear whether different residues on α1I are involved in binding to different collagen G*XX*GER motifs. If so, one could imagine that DXMS studies using α1I bound to individual THP units might be informative.

In contrast to collagen, binding of the function-blocking α1 antibody AQC2 led to much more limited changes in the DXMS pattern of α1I. In the crystal structure of the AQC2-α1I complex, Asp-101 from the antibody heavy chain bound directly to the metal ion in the α1I MIDAS, but the remainder of the I domain, including the C terminus, retained the closed conformation (30). We found that AQC2 binding selectively protected MIDAS loop 2, the same region protected from exchange by collagen. The similarity of AQC2 and collagen in their interactions with the metal ion and MIDAS loop 2, coupled with the stark differences in their abilities to transmit allosteric changes to the C terminus of α1I, is remarkable.

Two other examples of ligand-mimetic I domain antibodies have been reported, both of which also present Asp residues that interact with the MIDAS metal ion. One of these is the αL antibody AL-57 (76). Unlike AQC2, AL-57 binds to the open form of αL (68). It was suggested that a key salt bridge formed with Glu-241 of αL by either the native ligand ICAM-1 or AL-57 is necessary for the allosteric rearrangement to occur and that the reason AQC2 binds to the open form of α1I is that it does not form a similar bridge with the corresponding residue in α1I, Glu-255 (68). Unlike in the αL-ICAM interaction, this conserved glutamic acid (Glu-255 in α1 or Glu-256 in α2) is not critical for collagen binding by integrins (6, 67). Nonetheless, the finding that collagen but not AQC2 can induce long range conformational changes in α1I is consistent with the conclusion that AL-57 is a true ligand mimetic, whereas AQC2 co-opts a key element of the ligand-binding site (*i.e.* the MIDAS cation) without engaging other regions necessary for induction of signaling. One would predict that solution DXMS studies using AL-57 and the αL I domain should demonstrate pronounced antibody-induced conformational changes in the α7 helix. A true ligand-mimetic antibody would be less desirable as a therapeutic, however, because it could lead to agonistic effects through outside-in integrin signaling. Another related antibody, mAb107, preferentially binds to the αM I domain in Ca^{2+} via a bidentate interaction with Asp-107 (61, 77). Similarly to AQC2, ligation of mAb107 did not induce conversion to the open conformation. Interestingly, the bidentate mode of binding led to a heptavalent Ca^{2+} ion in the mAb107-I domain complex, highlighting the range of different geometries accessible by the MIDAS.

In summary, we have explored the dynamic conformational changes in the α1 integrin I domain induced by divalent cations and by ligand binding, and we tested several elements of the existing models for collagen-induced conformational changes and allosteric regulation, using DXMS. The data validated some elements of the models derived from crystallographic studies but importantly identified novel features of ligand and metal ion binding that were not detected using static methods. The application of DXMS to other integrin/ligand interactions should be very powerful, as it provides a method to explore the interaction of isolated I domains or even complete integrin heterodimers with native ligands, and it does not require the use of either conformationally restricted integrins (*e.g.* locked-open I domains) or engineered fragments of ligands (*e.g.* collagen THPs or RGD peptides).

Acknowledgments—We thank Mia Rushe for purification of the α1 I domain and Paul Rayhorn for experimental assistance and helpful discussions.

REFERENCES

1. Luo, B. H., Carman, C. V., and Springer, T. A. (2007) Structural basis of integrin regulation and signaling. *Annu. Rev. Immunol.* **25,** 619–647
2. Takagi, J. (2007) Structural basis for ligand recognition by integrins. *Curr. Opin. Cell Biol.* **19,** 557–564
3. Shimaoka, M., Xiao, T., Liu, J. H., Yang, Y., Dong, Y., Jun, C. D., McCormack, A., Zhang, R., Joachimiak, A., Takagi, J., Wang, J. H., and Springer, T. A. (2003) Structures of the αL I domain and its complex with ICAM-1 reveal a shape-shifting pathway for integrin regulation. *Cell* **112,** 99–111
4. Song, G., Yang, Y., Liu, J. H., Casasnovas, J. M., Shimaoka, M., Springer, T. A., and Wang, J. H. (2005) An atomic resolution view of ICAM recognition in a complex between the binding domains of ICAM-3 and integrin αLβ2. *Proc. Natl. Acad. Sci. U.S.A.* **102,** 3366–3371
5. Zhang, H., Casasnovas, J. M., Jin, M., Liu, J. H., Gahmberg, C. G., Springer, T. A., and Wang, J. H. (2008) An unusual allosteric mobility of the C-terminal helix of a high affinity αL integrin I domain variant bound to ICAM-5. *Mol. Cell* **31,** 432–437
6. Emsley, J., Knight, C. G., Farndale, R. W., Barnes, M. J., and Liddington, R. C. (2000) Structural basis of collagen recognition by integrin α2β1. *Cell* **101,** 47–56
7. Hynes, R. O. (2002) Integrins. Bidirectional, allosteric signaling machines. *Cell* **110,** 673–687
8. Huth, J. R., Olejniczak, E. T., Mendoza, R., Liang, H., Harris, E. A., Lupher, M. L., Jr., Wilson, A. E., Fesik, S. W., and Staunton, D. E. (2000) NMR and mutagenesis evidence for an I domain allosteric site that regulates lymphocyte function-associated antigen 1 ligand binding. *Proc. Natl. Acad. Sci. U.S.A.* **97,** 5231–5236
9. Shimaoka, M., Salas, A., Yang, W., Weitz-Schmidt, G., and Springer, T. A. (2003) Small molecule integrin antagonists that bind to the β2 subunit I-like domain and activate signals in one direction and block them in the other. *Immunity* **19,** 391–402
10. Legge, G. B., Kriwacki, R. W., Chung, J., Hommel, U., Ramage, P., Case, D. A., Dyson, H. J., and Wright, P. E. (2000) NMR solution structure of the inserted domain of human leukocyte function associated antigen-1. *J. Mol. Biol.* **295,** 1251–1264
11. Qu, A., and Leahy, D. J. (1996) The role of the divalent cation in the structure of the I domain from the CD11a/CD18 integrin. *Structure* **4,** 931–942
12. Lee, J. O., Rieu, P., Arnaout, M. A., and Liddington, R. (1995) Crystal structure of the A domain from the α subunit of integrin CR3 (CD11b/CD18). *Cell* **80,** 631–638
13. Li, R., Rieu, P., Griffith, D. L., Scott, D., and Arnaout, M. A. (1998) Two functional states of the CD11b A-domain. Correlations with key features of two Mn^{2+}-complexed crystal structures. *J. Cell Biol.* **143,** 1523–1534
14. Xie, C., Zhu, J., Chen, X., Mi, L., Nishida, N., and Springer, T. A. (2010) Structure of an integrin with an αI domain, complement receptor type 4. *EMBO J.* **29,** 666–679
15. Alonso, J. L., Essafi, M., Xiong, J. P., Stehle, T., and Arnaout, M. A. (2002) Does the integrin αA domain act as a ligand for its βA domain? *Curr. Biol.* **12,** R340–R342
16. Yang, W., Shimaoka, M., Salas, A., Takagi, J., and Springer, T. A. (2004) Intersubunit signal transmission in integrins by a receptor-like interaction with a pull spring. *Proc. Natl. Acad. Sci. U.S.A.* **101,** 2906–2911
17. Duband, J. L., Belkin, A. M., Syfrig, J., Thiery, J. P., and Koteliansky, V. E. (1992) Expression of α1 integrin, a laminin-collagen receptor, during

myogenesis and neurogenesis in the avian embryo. *Development* **116,** 585–600
18. Abraham, W. M., Ahmed, A., Serebriakov, I., Carmillo, A. N., Ferrant, J., de Fougerolles, A. R., Garber, E. A., Gotwals, P. J., Koteliansky, V. E., Taylor, F., and Lobb, R. R. (2004) A monoclonal antibody to $\alpha1\beta1$ blocks antigen-induced airway responses in sheep. *Am. J. Respir. Crit. Care Med.* **169,** 97–104
19. Chen, L., Huq, S., Gardner, H., de Fougerolles, A. R., Barabino, S., and Dana, M. R. (2007) Very late antigen 1 blockade markedly promotes survival of corneal allografts. *Arch. Ophthalmol.* **125,** 783–788
20. Cosgrove, D., Rodgers, K., Meehan, D., Miller, C., Bovard, K., Gilroy, A., Gardner, H., Kotelianski, V., Gotwals, P., Amatucci, A., and Kalluri, R. (2000) Integrin $\alpha1\beta1$ and transforming growth factor-$\beta1$ play distinct roles in alport glomerular pathogenesis and serve as dual targets for metabolic therapy. *Am. J. Pathol.* **157,** 1649–1659
21. de Fougerolles, A. R., Chi-Rosso, G., Bajardi, A., Gotwals, P., Green, C. D., and Koteliansky, V. E. (2000) Global expression analysis of extracellular matrix/integrin interactions in monocytes. *Immunity* **13,** 749–758
22. Ianaro, A., Cicala, C., Calignano, A., Koteliansky, V., Gotwals, P., Bucci, M., Gerli, R., Santucci, L., Fiorucci, S., and Cirino, G. (2000) Anti-very late antigen-1 monoclonal antibody modulates the development of secondary lesion and T-cell response in experimental arthritis. *Lab. Invest.* **80,** 73–80
23. Krieglstein, C. F., Cerwinka, W. H., Sprague, A. G., Laroux, F. S., Grisham, M. B., Koteliansky, V. E., Senninger, N., Granger, D. N., and de Fougerolles, A. R. (2002) Collagen-binding integrin $\alpha1\beta1$ regulates intestinal inflammation in experimental colitis. *J. Clin. Invest.* **110,** 1773–1782
24. Meharra, E. J., Schön, M., Hassett, D., Parker, C., Havran, W., and Gardner, H. (2000) Reduced gut intraepithelial lymphocytes in VLA1 null mice. *Cell. Immunol.* **201,** 1–5
25. Ray, S. J., Franki, S. N., Pierce, R. H., Dimitrova, S., Koteliansky, V., Sprague, A. G., Doherty, P. C., de Fougerolles, A. R., and Topham, D. J. (2004) The collagen binding $\alpha1\beta1$ integrin VLA-1 regulates CD8 T cell-mediated immune protection against heterologous influenza infection. *Immunity* **20,** 167–179
26. Nolte, M., Pepinsky, R. B., Venyaminov, S. Yu., Koteliansky, V., Gotwals, P. J., and Karpusas, M. (1999) Crystal structure of the $\alpha\beta1$ integrin I-domain. Insights into integrin I-domain function. *FEBS Lett.* **452,** 379–385
27. Nymalm, Y., Puranen, J. S., Nyholm, T. K., Käpylä, J., Kidron, H., Pentikäinen, O. T., Airenne, T. T., Heino, J., Slotte, J. P., Johnson, M. S., and Salminen, T. A. (2004) Jararhagin-derived RKKH peptides induce structural changes in $\alpha1$I domain of human integrin $\alpha1\beta1$. *J. Biol. Chem.* **279,** 7962–7970
28. Rich, R. L., Deivanayagam, C. C., Owens, R. T., Carson, M., Höök, A., Moore, D., Symersky, J., Yang, V. W., Narayana, S. V., and Höök, M. (1999) Trench-shaped binding sites promote multiple classes of interactions between collagen and the adherence receptors, $\alpha_1\beta_1$ integrin and *Staphylococcus aureus* cna MSCRAMM. *J. Biol. Chem.* **274,** 24906–24913
29. Clark, L. A., Boriack-Sjodin, P. A., Eldredge, J., Fitch, C., Friedman, B., Hanf, K. J., Jarpe, M., Liparoto, S. F., Li, Y., Lugovskoy, A., Miller, S., Rushe, M., Sherman, W., Simon, K., and Van Vlijmen, H. (2006) Affinity enhancement of an *in vivo* matured therapeutic antibody using structure-based computational design. *Protein Sci.* **15,** 949–960
30. Karpusas, M., Ferrant, J., Weinreb, P. H., Carmillo, A., Taylor, F. R., and Garber, E. A. (2003) Crystal structure of the $\alpha1\beta1$ integrin I domain in complex with an antibody Fab fragment. *J. Mol. Biol.* **327,** 1031–1041
31. Saccà, B., Sinner, E. K., Kaiser, J., Lübken, C., Eble, J. A., and Moroder, L. (2002) Binding and docking of synthetic heterotrimeric collagen type IV peptides with $\alpha1\beta1$ integrin. *ChemBioChem* **3,** 904–907
32. Lahti, M., Bligt, E., Niskanen, H., Parkash, V., Brandt, A. M., Jokinen, J., Patrikainen, P., Käpylä, J., Heino, J., and Salminen, T. A. (2011) Structure of collagen receptor integrin α_1I domain carrying the activating mutation E317A. *J. Biol. Chem.* **286,** 43343–43351
33. Burke, J. E., Hsu, Y. H., Deems, R. A., Li, S., Woods, V. L., Jr., and Dennis, E. A. (2008) A phospholipid substrate molecule residing in the membrane surface mediates opening of the lid region in group IVA cytosolic phospholipase A_2. *J. Biol. Chem.* **283,** 31227–31236
34. Coales, S. J., Tuske, S. J., Tomasso, J. C., and Hamuro, Y. (2009) Epitope mapping by amide hydrogen/deuterium exchange coupled with immobilization of antibody, on-line proteolysis, liquid chromatography, and mass spectrometry. *Rapid Commun. Mass Spectrom.* **23,** 639–647
35. Engen, J. R. (2009) Analysis of protein conformation and dynamics by hydrogen/deuterium exchange MS. *Anal. Chem.* **81,** 7870–7875
36. Hamuro, Y., Coales, S. J., Hamuro, L. L., and Woods, V. L., Jr. (2008) in *Mass Spectrometry Analysis for Protein-Protein Interactions and Dynamics* (Chance, M., ed) pp. 123–155, Wiley-VCH, Hoboken, NJ
37. Hsu, Y. H., Burke, J. E., Li, S., Woods, V. L., Jr., and Dennis, E. A. (2009) Localizing the membrane binding region of Group VIA Ca^{2+}-independent phospholipase A_2 using peptide amide hydrogen/deuterium exchange mass spectrometry. *J. Biol. Chem.* **284,** 23652–23661
38. Konermann, L., Tong, X., and Pan, Y. (2008) Protein structure and dynamics studied by mass spectrometry. H/D exchange, hydroxyl radical labeling, and related approaches. *J. Mass. Spectrom.* **43,** 1021–1036
39. Mendillo, M. L., Hargreaves, V. V., Jamison, J. W., Mo, A. O., Li, S., Putnam, C. D., Woods, V. L., Jr., and Kolodner, R. D. (2009) A conserved MutS homolog connector domain interface interacts with MutL homologs. *Proc. Natl. Acad. Sci. U.S.A.* **106,** 22223–22228
40. Truhlar, S. M., Torpey, J. W., and Komives, E. A. (2006) Regions of IκBα that are critical for its inhibition of NF-κB. DNA interaction fold upon binding to NF-κB. *Proc. Natl. Acad. Sci. U.S.A.* **103,** 18951–18956
41. Gotwals, P. J., Chi-Rosso, G., Ryan, S. T., Sizing, I., Zafari, M., Benjamin, C., Singh, J., Venyaminov, S. Y., Pepinsky, R. B., and Koteliansky, V. (1999) Divalent cations stabilize the $\alpha1\beta1$ integrin I domain. *Biochemistry* **38,** 8280–8288
42. Weinreb, P. H., Yang, W. J., Violette, S. M., Couture, M., Kimball, K., Pepinsky, R. B., Lobb, R. R., and Josiah, S. (2002) A cell-free electrochemiluminescence assay for measuring $\beta1$-integrin-ligand interactions. *Anal. Biochem.* **306,** 305–313
43. Hamuro, Y., Zawadzki, K. M., Kim, J. S., Stranz, D. D., Taylor, S. S., and Woods, V. L., Jr. (2003) Dynamics of cAPK type IIβ activation revealed by enhanced amide $H/^2H$ exchange mass spectrometry (DXMS). *J. Mol. Biol.* **327,** 1065–1076
44. Burns-Hamuro, L. L., Hamuro, Y., Kim, J. S., Sigala, P., Fayos, R., Stranz, D. D., Jennings, P. A., Taylor, S. S., and Woods, V. L., Jr. (2005) Distinct interaction modes of an AKAP bound to two regulatory subunit isoforms of protein kinase A revealed by amide hydrogen/deuterium exchange. *Protein Sci.* **14,** 2982–2992
45. Hamuro, Y., Anand, G. S., Kim, J. S., Juliano, C., Stranz, D. D., Taylor, S. S., and Woods, V. L., Jr. (2004) Mapping intersubunit interactions of the regulatory subunit (RIα) in the type I holoenzyme of protein kinase A by amide hydrogen/deuterium exchange mass spectrometry (DXMS). *J. Mol. Biol.* **340,** 1185–1196
46. Pantazatos, D., Kim, J. S., Klock, H. E., Stevens, R. C., Wilson, I. A., Lesley, S. A., and Woods, V. L., Jr. (2004) Rapid refinement of crystallographic protein construct definition employing enhanced hydrogen/deuterium exchange MS. *Proc. Natl. Acad. Sci. U.S.A.* **101,** 751–756
47. Spraggon, G., Pantazatos, D., Klock, H. E., Wilson, I. A., Woods, V. L., Jr., and Lesley, S. A. (2004) On the use of DXMS to produce more crystallizable proteins. Structures of the *T. maritima* proteins TM0160 and TM1171. *Protein Sci.* **13,** 3187–3199
48. Zhang, Z., and Smith, D. L. (1993) Determination of amide hydrogen exchange by mass spectrometry. A new tool for protein structure elucidation. *Protein Sci.* **2,** 522–531
49. Hsu, S., Kim, Y., Li, S., Durrant, E. S., Pace, R. M., Woods, V. L., Jr., and Gentry, M. S. (2009) Structural insights into glucan phosphatase dynamics using amide hydrogen-deuterium exchange mass spectrometry. *Biochemistry* **48,** 9891–9902
50. Hsu, Y. H., Burke, J. E., Stephens, D. L., Deems, R. A., Li, S., Asmus, K. M., Woods, V. L., Jr., and Dennis, E. A. (2008) Calcium binding rigidifies the C2 domain and the intradomain interaction of GIVA phospholipase A_2 as revealed by hydrogen/deuterium exchange mass spectrometry. *J. Biol. Chem.* **283,** 9820–9827
51. Bai, Y., Milne, J. S., Mayne, L., and Englander, S. W. (1993) Primary structure effects on peptide group hydrogen exchange. *Proteins* **17,** 75–86
52. Molday, R. S., Englander, S. W., and Kallen, R. G. (1972) Primary structure effects on peptide group hydrogen exchange. *Biochemistry* **11,** 150–158
53. Oyeyemi, O. A., Sours, K. M., Lee, T., Resing, K. A., Ahn, N. G., and

Klinman, J. P. (2010) Temperature dependence of protein motions in a thermophilic dihydrofolate reductase and its relationship to catalytic efficiency. *Proc. Natl. Acad. Sci. U.S.A.* **107,** 10074–10079
54. Wilderman, P. R., Shah, M. B., Liu, T., Li, S., Hsu, S., Roberts, A. G., Goodlett, D. R., Zhang, Q., Woods, V. L., Jr., Stout, C. D., and Halpert, J. R. (2010) Plasticity of cytochrome P450 2B4 as investigated by hydrogen-deuterium exchange mass spectrometry and x-ray crystallography. *J. Biol. Chem.* **285,** 38602–38611
55. Sali, A., and Blundell, T. L. (1993) Comparative protein modeling by satisfaction of spatial restraints. *J. Mol. Biol.* **234,** 779–815
56. Eswar, N., Webb, B., Marti-Renom, M. A., Madhusudhan, M. S., Eramian, D., Shen, M. Y., Pieper, U., and Sali, A. (2007) in *Current Protocols in Protein Science* (Colligan, J. E., Dunn, B. M., Speicher, D.W., and Wingfield, P.T., eds) pp. 2.9.1–2.9.31, Wiley Interscience, Hoboken, NJ
57. Chasseaud, L. F. (1979) The role of glutathione and glutathione *S*-transferases in the metabolism of chemical carcinogens and other electrophilic agents. *Adv. Cancer Res.* **29,** 175–274
58. Calderwood, D. A., Tuckwell, D. S., Eble, J., Kühn, K., and Humphries, M. J. (1997) The integrin α1A-domain is a ligand-binding site for collagens and laminin. *J. Biol. Chem.* **272,** 12311–12317
59. Dickeson, S. K., Mathis, N. L., Rahman, M., Bergelson, J. M., and Santoro, S. A. (1999) Determinants of ligand binding specificity of the $\alpha_1\beta_1$ and $\alpha_2\beta_1$ integrins. *J. Biol. Chem.* **274,** 32182–32191
60. Luque, A., Sánchez-Madrid, F., and Cabañas, C. (1994) Functional regulation of the human integrin VLA-1 (CD49a/CD29) by divalent cations and stimulatory β1 antibodies. *FEBS Lett.* **346,** 278–284
61. Ajroud, K., Sugimori, T., Goldmann, W. H., Fathallah, D. M., Xiong, J. P., and Arnaout, M. A. (2004) Binding affinity of metal ions to the CD11b A-domain is regulated by integrin activation and ligands. *J. Biol. Chem.* **279,** 25483–25488
62. Baldwin, E. T., Sarver, R. W., Bryant, G. L., Jr., Curry, K. A., Fairbanks, M. B., Finzel, B. C., Garlick, R. L., Heinrikson, R. L., Horton, N. C., Kelley, L. L., Mildner, A. M., Moon, J. B., Mott, J. E., Mutchler, V. T., Tomich, C. S., Watenpaugh, K. D., and Wiley, V. H. (1998) Cation binding to the integrin CD11b I domain and activation model assessment. *Structure* **6,** 923–935
63. Michishita, M., Videm, V., and Arnaout, M. A. (1993) A novel divalent cation-binding site in the A domain of the β_2 integrin CR3 (CD11b/CD18) is essential for ligand binding. *Cell* **72,** 857–867
64. Liddington, R., and Bankston, L. (1998) The integrin I domain. Crystals, metals, and related artifacts. *Structure* **6,** 937–938
65. Bella, J., and Berman, H. M. (2000) Integrin-collagen complex. A metal-glutamate handshake. *Structure* **8,** R121–126
66. Tu, T., Drăguşanu, M., Petre, B. A., Rempel, D. L., Przybylski, M., and Gross, M. L. (2010) Protein-peptide affinity determination using an h/d exchange dilution strategy. Application to antigen-antibody interactions. *J. Am. Soc. Mass Spectrom.* **21,** 1660–1667
67. Kamata, T., Liddington, R. C., and Takada, Y. (1999) Interaction between collagen and the α_2 I-domain of integrin $\alpha_2\beta_1$. Critical role of conserved residues in the metal ion-dependent adhesion site (MIDAS) region. *J. Biol. Chem.* **274,** 32108–32111
68. Zhang, H., Liu, J. H., Yang, W., Springer, T., Shimaoka, M., and Wang, J. H. (2009) Structural basis of activation-dependent binding of ligand-mimetic antibody AL-57 to integrin LFA-1. *Proc. Natl. Acad. Sci. U.S.A.* **106,** 18345–18350
69. Chen, J., Takagi, J., Xie, C., Xiao, T., Luo, B. H., and Springer, T. A. (2004) The relative influence of metal ion-binding sites in the I-like domain and the interface with the hybrid domain on rolling and firm adhesion by integrin α4β7. *J. Biol. Chem.* **279,** 55556–55561
70. Griggs, D. W., Schmidt, C. M., and Carron, C. P. (1998) Characteristics of cation binding to the I domains of LFA-1 and MAC-1. The LFA-1 I domain contains a Ca^{2+}-binding site. *J. Biol. Chem.* **273,** 22113–22119
71. San Sebastian, E., Mercero, J. M., Stote, R. H., Dejaegere, A., Cossío, F. P., and Lopez, X. (2006) On the affinity regulation of the metal-ion-dependent adhesion sites in integrins. *J. Am. Chem. Soc.* **128,** 3554–3563
72. Obsil, T., Hofbauerová, K., Amler, E., and Teisinger, J. (1999) Different cation binding to the I domains of α1 and α2 integrins. Implication of the binding site structure. *FEBS Lett.* **457,** 311–315
73. Käpylä, J., Ivaska, J., Riikonen, R., Nykvist, P., Pentikäinen, O., Johnson, M., and Heino, J. (2000) Integrin α_2I domain recognizes type I and type IV collagens by different mechanisms. *J. Biol. Chem.* **275,** 3348–3354
74. Lambert, L. J., Bobkov, A. A., Smith, J. W., and Marassi, F. M. (2008) Competitive interactions of collagen and a jararhagin-derived disintegrin peptide with the integrin α2-I domain. *J. Biol. Chem.* **283,** 16665–16672
75. Siljander, P. R., Hamaia, S., Peachey, A. R., Slatter, D. A., Smethurst, P. A., Ouwehand, W. H., Knight, C. G., and Farndale, R. W. (2004) Integrin activation state determines selectivity for novel recognition sites in fibrillar collagens. *J. Biol. Chem.* **279,** 47763–47772
76. Shimaoka, M., Kim, M., Cohen, E. H., Yang, W., Astrof, N., Peer, D., Salas, A., Ferrand, A., and Springer, T. A. (2006) AL-57, a ligand-mimetic antibody to integrin LFA-1, reveals chemokine-induced affinity up-regulation in lymphocytes. *Proc. Natl. Acad. Sci. U.S.A.* **103,** 13991–13996
77. Mahalingam, B., Ajroud, K., Alonso, J. L., Anand, S., Adair, B. D., Horenstein, A. L., Malavasi, F., Xiong, J. P., and Arnaout, M. A. (2011) Stable coordination of the inhibitory Ca^{2+} ion at the metal ion-dependent adhesion site in integrin CD11b/CD18 by an antibody-derived ligand aspartate. Implications for integrin regulation and structure-based drug design. *J. Immunol.* **187,** 6393–6401